NASA Contractor Report 185122

Theoretical Studies in Support of the 3M-Vapor Transport (PVTOS-) Experiments

Daniel E. Rosner and David E. Keyes
Yale University
New Haven, Connecticut

July 1989

Prepared for
Lewis Research Center
Under Grant NAG3-898

National Aeronautics and
Space Administration

TABLE OF CONTENTS

PAGE

THEORETICAL STUDIES IN SUPPORT OF THE 3M-VAPOR TRANSPORT (PVTOS-) EXPERIMENTS

NASA Grant NAG 3-898
FINAL REPORT

prepared by
DANIEL E. ROSNER and DAVID E. KEYES
Yale University, New Haven, CT 06520, U.S.A.

ABSTRACT

Results are reported of a preliminary theoretical study of the coupled mass-, momentum-, and heat-transfer conditions expected within small ampoules used to grow oriented organic solid (OS-) films, by physical vapor transport (PVT) in microgravity environments. It is shown that previous studies made restrictive assumptions (*e.g.*, smallness of $\Delta T/T$, equality of molecular diffusivities) *not* valid under PVTOS conditions, whereas the important phenomena of sidewall gas 'creep', Soret transport of the organic vapor, and large vapor phase supersaturations associated with the large prevailing temperature gradients were not previously considered. Rational estimates are made of the molecular transport properties relevant to copper-phthalocyanine monomeric vapor in a gas mixture containing H_2(g) and Xe(g). Efficient numerical methods have been developed and are outlined/illustrated here for making steady axisymmetric gas flow calculations within such ampoules, allowing for realistic $\Delta T/T_w$-values, and even corrections to Navier-Stokes-Fourier 'closure' for the governing 'continuum' differential equations. High priority follow-on studies are outlined based on these new results.

December 1988

1. INTRODUCTION

1.1 Implications of PVTOS-1 Experiments: Important Questions

Based on a preliminary review meeting, 16 December 1987, at NASA Lewis Lab, our critical review of T.L. Miller's preliminary numerical calculations (Miller, 1986) and recent PVT, CVD-research at the Yale University HTCRE Laboratory (Rosner, 1980, 1985, 1986, 1988; and Garcia-Ybarra and Rosner, 1988) we embarked on a pilot theoretical study to gain an understanding of why microgravity-grown organic films (Space Shuttle Orbiter) are frequently of higher quality (*e.g.*, in terms of smoothness, optical homogeneity, and degree of uniaxial orientation) than those grown at ± 1 g (earth). The results of this pilot study (7 April - 31 August 1988) are reported here, with emphasis on those important thermophysical phenomena neglected in earlier quantitative discussions of ampoule PVT-experiments (see, *e.g.*, Section 1.3). Please note that the parameters assumed (or assigned) in the illustrative calculations which follow should not be taken to be best current estimates based on actual measurements made during previous PVTOS experiments on space shuttle flights. They are, instead, rough numbers chosen to illustrate our *procedures*, and to assess the relative importance of competing effects.

1.2 Previous Theoretical Studies: Natural Convection in PVT-Ampoules

It is well-known that even in outwardly simple, closed ampoules, rather complex vapor flows can occur due to the effects of a body force (usually gravity; see, *e.g.*, Ostrach, 1982) and/or induced by the mass transfer process itself (Stefan flow) — see, *e.g.*, Rosenberger, 1979; and Rosner, 1966. These have been analyzed in simple situations (ampoule geometry, ampoule orientation with respect to gravity, small fractional change in mixture density, equal vapor diffusivities for the transport of momentum, heat and mass, no-slip wall boundary conditions, no side-wall effects, ...), with a typical set of results reported in Miller, 1986. We show below (Sections 1.3, 2) that these earlier studies, ironically, emphasize phenomena *not* important under 3M-PVTOS-experimental conditions (Stefan flow, effect of organic vapor concentration on vapor mixture density), but neglect several phenomena which *are* likely to be important under such conditions ("creep" along nonisothermal ampoule side-walls, Soret transport of vapor, unequal molecular diffusivities, side-wall scavenging of heat and/or vapor mass, vapor clustering in the prevailing supersaturation field near the vapor/solid film interface). One of our goals is to converge on the simplest thermophysical model which includes all of the essential phenomena operating under 3M-PVTOS conditions, with emphasis on their crystal quality implications.

1.3 Identification of Important, Yet Previously Neglected Thermophysical Phenomena: Summary of Present Report

Using a series of quantitative estimates based on relevant *ratios* (*i.e.*, dimensionless groups) evaluated under conditions relevant to past and future 3M-PVTOS experiments, we systematically evaluate in Section 2 the relative importance of a variety of thermophysical phenomena, many previously explicitly or implicitly neglected despite their likely importance in the 3M-PVTOS context. As a result of the present pilot program, we have discovered and initiated exploration of the roles of:

- Soret transport of heavy organic vapors in the nonisothermal (low molecular weight) background gas (Section 2.1)
- Soret separation of the background gas mixture in the prevailing temperature gradient (Section 2.2)
- Gas "creep" (non-zero "slip") along the ampoule side-walls — an important 'cause' of convection independent of gravity (Section 2.4.3)
- Unequal molecular diffusivities for the transport of momentum, heat, and vapor mass (effects of low mixture Prandtl number and high vapor Schmidt number (Section 2.3)
- Vapor phase supersaturations (and organic vapor clustering?) near the vapor/OS interface (Section 2.5)
- Departures from the Boussinesq (small mixture density change) approximation (Section 3.2)
- Role of ampoule side-wall losses of heat and organic vapor mass (Section 3.8)
- Breakdown of the Navier-Stokes field equations (need for Burnett terms; Section 2.5)

To the extent possible in this pilot program, we also outline in Sections 2, 3, 4 how these phenomena can be included and what film growth effects they are likely to have, *via* illustrative predictions whenever possible (Sections 3, 4). In the course of these evaluations, we also are able to defend certain simplifications previously made for convenience (*e.g.*, vapor/solid equilibrium at the vapor/film interface; Section 2.4.2) and define the growth conditions under which they are likely to fail. Perhaps more important, we pinpoint presently missing information and/or theoretical advances which should be the focus of follow-on PVTOS studies. In view of the expense of microgravity experiments there is clearly an enormous incentive to gain the theoretical understanding necessary to optimize the design of both microgravity and ground-based experiments, perhaps, even simulating the 'benefits' of microgravity in future ground-based deposition equipment.

2. PHYSICO-CHEMICAL MODELING

2.1 Soret Effect and Soret Coefficient for 'CuPc' Transport

As discussed in greater detail in Rosner (1980, 1988), heavy particle transport toward a cooler surface can be accelerated appreciably by the phenomenon of Soret transport (for vapors) or 'thermophoresis' (for *bona fide* particles). In dilute mixtures this is described by a generalized diffusion flux law of the additive form:

$$\underset{\text{Fick}}{\mathbf{j}_v''} = D_v \rho (-\mathbf{grad}\, \omega_v) + \underset{\text{Soret}}{\alpha_T D_v \rho \omega_v (-\mathbf{grad}\, (\ln T))} \qquad (2.1\text{-}1)$$

where α_T is the (dimensionless) Soret factor and the remaining terms are defined in Section 7. Available theory and measurements for α_T pertain to 'quasi-spherical' molecules in low density gases, however, it is possible to invoke gas kinetic theory to estimate the values of α_T (and D_v) in the PVTOS-ampoule environment. For a nonconvective gas film across which there is a temperature difference ΔT Rosner (1980) has shown that mass transfer augmentations due to this cause will be of the order of:

$$F\{B_T\} \approx \frac{B_T}{\exp\{B_T\} - 1} \qquad (2.1\text{-}2)$$

where

$$B_T \cong \frac{-\alpha_T \Delta T}{T_w} \qquad (2.1\text{-}3)$$

(A more exact approach is described in Section 4.)

Depending on the method of estimation and the nature of the background gas chosen we obtain values of α_T in the approximate range 2 (for CuPc(v) in the gas mixture discussed in Section 2.3) to about 10 for CuPc(v) in pure helium. But even taking the lower value and inserting

$$\frac{(T_e - T_w)}{T_w} \cong \frac{(673 - 510)\,K}{510\,K} = \frac{163}{510} \cong 0.32$$

we find $B_T \cong -0.58$ and $F\{B_T\} \cong 1.32$ corresponding to about a 32 percent systematic augmentation in PVT-*rate* due to Soret transport. Moreover, as shown in Section 4.7, Soret transport influences expected *vapor supersaturations* near the deposition surface (which may influence deposit morphology) and, as shown in Section 2.2, there will be a systematic Soret-induced segregation in the composition of the effective 'carrier gas' which, in turn, can contribute to the gas 'creep' along the ampoule side-walls (Section 2.4.3). Accordingly, we conclude that future theoretical studies in support of the PVTOS experiments should include the systematic effects of CuPc(g) *Soret* transport, and develop improved methods for estimating α_T for 'sheet-

like' macro-molecules based on extensions of available kinetic theory* and available structural information for polycyclic macromolecules like CuPc (Brown, 1968). In the *illustrative* calculations reported in Section 4 the coefficient α_T has been considered an 'assignable' parameter taking on values between 0 (no Soret effect) and 10 (maximum Soret effect). The latter case will be seen to correspond to Soret PVT-rate enhancements of about 3-fold when $T_e/T_w \approx 673\ K/510\ K = 1.32$ and, as much as 5-fold when $T_e/T_w \approx 673\ K/345\ K = 1.95$.

2.2 Soret-Induced Separation in the Carrier Gas Mixture

Since the 'background' gas in the PVT-ampoule can contain gases of widely disparate molecular weight (*e.g.*, Xe [M=131.3] and H_2 [M=2.016]) the abovementioned Soret effect will cause a steady-state 'segregation' phenomenon in the ampoule background gas (Rosner, 1980). The tendency of the heavier constituent to be thermally driven toward the 'cold' (deposition) surface will give rise to a Xe-concentration enrichment there, the magnitude of which is readily estimated in the absence of convective flow (*i.e.* when the Fick flux and Soret Flux are equal but opposed in direction). For the 'worst case' of xenon dilute in hydrogen and at a temperature ratio Te/Tw of, say, (673 K/510 K) = 1.32, we estimate below that this phenomenon would cause about a 17 percent change in the Xe composition across the cell. As a corollary of this effect, concentration gradients will also make a contribution to the gas mixture 'creep' velocity along the sidewalls (*e.g.*, Kramers and Kistemaker, 1943) — even in the absence of gravity. The background gas Soret segregation effect will, of course, become less important in the case of lighter inert gas constituents (*e.g.*, Kr, Ar, Ne, He) since the thermal diffusion factor α_T appearing in Eqs 2.1-1, 3 and 2.2-1 (below) diminishes with the molecular weight disparity parameter $r \equiv (M_i - M_j)/(M_i + M_j)$ (Rosner, 1980, 1985).

To illustrate the extent of the 'background' gas Soret segregation, we note that when the Soret flux counterbalances the Fick flux (Rosner, 1980)

$$\frac{\omega_{Xe}(T_{cold})}{\omega_{Xe}(T_{hot})} \cong \left(\frac{T_{hot}}{T_{cold}}\right)^{\alpha_T} \qquad (2.2\text{-}1)$$

Using the kinetic theory estimation methods described in Rosner (1980, 1985, 1988), we estimate the α_T near 600 K would be about 0.58 for this (Xe/H_2) system. Inserting the temperature ratio $T_e/T_w \cong (673\ K/510\ K) = 1.32$ gives the abovementioned 17 percent background gas segregation effect. On this basis, for the remainder of our present estimates, this segregation will be neglected,

---

* A rational method to predict α_T-values for slowly tumbling nonspherical molecules in a light gas (mixture) has recently been developed by Garcia-Ybarra and Rosner (1988). However, in the present case, analogous methods are needed for rapidly tumbling nonspherical molecules (Garcia-Ybarra and Rosner, 1988)

but it should be kept in mind in case future PVTOS is done at absolute temperature ratios much larger than 1.3, as is often the case.

2.3 Momentum, Heat and Mass Transfer Diffusivity Ratios (Pr, Sc)

There are three molecular diffusivities of considerable interest in predicting PVT-ampoule transport, *viz.* the *momentum* diffusivity $\nu \equiv \mu/\rho$,the *heat* diffusivity $\alpha_h \equiv k/(\rho c_p)$, and the CuPc vapor Fick *mass*-diffusivity D_v. Two important diffusivity *ratios* are therefore:

$$\frac{\nu}{\alpha_h} \equiv \mathrm{Pr} \qquad \text{(Prandtl number)} \qquad (2.3\text{-}1)$$

$$\frac{\nu}{D_v} \equiv \mathrm{Sc} \qquad \text{(Schmidt number)} \qquad (2.3\text{-}2)$$

In many situations involving momentum, energy and mass transport in 'simple' low density gases, the abovementioned molecular diffusivities are close to one another (J.C. Maxwell), causing the ratios Pr *and* Sc to be near unity. Indeed, for simplicity, T.C. Miller (1986) adopted Pr=Sc=1 in his PVT natural convection simulations. However, in the present PVTOS-ampoules we encounter gas mixtures containing molecules of widely disparate molecular weights (and size), *e.g.*, H_2, Xe and CuPc (M=575.67) — see Table 2.3-1, causing Pr and Sc to depart significantly from unity. Indeed, for the gas mixture defined in Table 2.3-1, using standard "rules" for the *mixture* properties μ, k (Rosner, 1986) and a rough estimate for the Fick diffusivity of CuPc(v) in this mixture (see below) we tentatively conclude that $\mathrm{Pr} \approx 0.37$ and $\mathrm{Sc} \approx 3.7$, showing that the diffusivities D_v and α_h can differ in PVTOS application by as much as about one order-of-magnitude (*i.e.* $D_v/\alpha_h \equiv \mathrm{Le} \approx .10$). This large a disparity between the CuPc(v) mass- and mixture heat diffusivities will inevitably have a strong influence on the comparative vapor pressure and temperature distributions, which, in turn, will dramatically influence vapor supersaturations in the vicinity of the vapor/OS-surface and, hence, perhaps, surface morphology (see Section 2.5). It will be absolutely essential to account for unequal molecular diffusivities in future PVTOS simulations (see Section 3).

Table 2.3-1

Constituent Properties[a] in a Typical PVTOS Background Gas Mixture[b,c]; T≈600K

Species	y_i	M_i	$10^6\mu_i$	10^6k_i	$C_{p,i}/R$
H_2	0.375	2.016	142.0	714.7	3.527
CO	0.125	28.01	289.8	108.6	3.661
CO_2	0.375	44.01	271.4	97.2	5.669
Xe	0.125	131.3	430.2	24.4	2.500

a Viscosities (g cm^{-1} s^{-1}), thermal conductivities (cal cm^{-1} s^{-1} K^{-1}) and (dimensionless) molar heat capacities are taken from the compilation of Svehla (1962)

b For this mixture at 3.2 Torr, 600 K, we estimate $\nu \approx 96$ cm^2/s, $\alpha_h \approx 260$ cm^2/s

c The mean molecular weight ($\Sigma\, y_i\, M_i$) of this mixture is 37.2

Pending development of more accurate methods (Garcia-Ybarra and Rosner, 1989), our estimate for D_v is based on the observation that the diffusivity of the nonspherical molecule CuPc(v) will probably be comparable to the diffusivity of a spherical molecule of equal volume (and mass), corrected by a weak function of nonsphericity (see, *e.g.*, Friedlander's summary (1977) of the earlier calculations of Perrin for ellipsoidal particles). For CuPc(v) with an estimated volume of 341Å^3 in the mixture considered in Table 2.3-1, we thereby estimate $D_v \approx 26$ cm^2/s at p=3.2 Torr, T=600 K. The disproportionate contribution to the thermal diffusivity of this gaseous mixture associated with H_2(g), and the large effective cross-section of CuPc(v) thus combine to produce a diffusivity disparity (D_v, cf. α_h) of about one order-of-magnitude.

2.4 Boundary Conditions

2.4.1 Stefan flow in PVTOS ampoules

In general, there is a convection towards any surface which is the site of a net deposition for non-dilute PVD and CVD-systems (see, *e.g.*, Rosner, 1966, 1986). While Miller (1986) has emphasized the consequences of this inevitable flow in his illustrative natural convection simulations, it is easy to show (below) that this phenomenon plays a ***negligible*** role in typical PVTOS experiments, *e.g.*, CuPc(v) growth under microgravity or ground-based conditions. This can be traced to the fact that even at the 'hot' boundary © the *equilibrium mass fraction* $\omega_{v,c;eq}$ of CuPc(v) is typically less than 0.4 percent, which also shows that *density* changes in such PVT-

ampoule mixtures will be due primarily to *temperature* changes, not changes in the CuPc(v) "solute" *concentration.*

As summarized, *e.g.*, in Rosner (1986), it is known that Stefan flow effects in simple systems are governed by the dimensionless "suction" parameter:

$$-B_{Stefan} \equiv \frac{\omega_{v,e} - \omega_{v,w}}{1 - \omega_{v,w}} \tag{2.4-1}$$

and deposition rate augmentation factors associated with this effect are of the order of:

$$\frac{-\dot{m}''_{v,w}}{(-\dot{m}_{v,w})_{Stefan\text{-}free}} \approx \frac{\ln(1 + B_{Stefan})}{B_{Stefan}} \tag{2.4-2}$$

If we now tentatively assume VSE at stations ⓔ and ⓦ (cf. Section 2.4.2) then:

$$\omega_{v,e} \cong \omega_{v,eq}\{T_e;p\} \tag{2.4-3a}$$

$$\omega_{v,w} \cong \omega_{v,eq}\{T_w;p\} \tag{2.4-3b}$$

Using the CuPc equilibrium vapor pressure law (see, also, Bonderman *et al.*, 1970):

$$\log_{10} p_{CuPc,eq}(atm) = -\frac{13661}{T} + 14.315 \tag{2.4-4}$$

we find that in the mixture defined in Section 2.3 when $T_e = 673$ K, $T_w = 510$ K,

$$\omega_{v,e} \approx 3.8 \times 10^{-3};\ \omega_{v,w} << \omega_{v,e};\ \text{and}\ \frac{-\dot{m}''_{v,w}}{(-\dot{m}_{v,w})_{Stefan\text{-}free}} \approx 1.002$$

At stil lower surface temperatures the Stefan flow effect is therefore even less than 0.2 percent.

2.4.2 Extent of Departures from Vapor/solid equilibrium (VSE) @ station ⓦ

Despite the fact that evaporation coefficients, α_{evap}, for CuPc have been reported to be as low as *ca.* 10^{-2} (see the summary of Bonderman *et al*, 1970), it can be shown that departures from VSE at the vapor/OS film boundary will be small compared to CuPc(v) concentration differences across the ampoule of height L. Thus, in the steady-state without appreciable convection, it can be shown that

$$\frac{\omega_{v,w} - \omega_{v,eq}\{T_w;p\}}{\omega_{v,e} - \omega_{v,w}}$$

will be small provided the dimensionless group

$$Dam_{het} \equiv \frac{\alpha_{cond} \cdot \left(\frac{1}{4}\bar{c}_{v,w}\right)L}{D_{v,mix}} \tag{2.4-5}$$

is of the order 10 or larger (see, *e.g.*, Rosner *et al.*, 1979). Here α_{cond} is the vapor condensation coefficient and $\bar{c}_{v,w}$ is the mean thermal speed of vapor molecules evaluated at the surface temperature T_w, *i.e.*:

$$\bar{c}_{v,w} = \left(\frac{8\,k_B\,T_w}{\pi m_v}\right)^{\frac{1}{2}} \tag{2.4-6}$$

It is reasonable to assume $\alpha_{cond} \approx \alpha_{evap} = 10^{-2}$, and evaluating Eq. (2.4-5) @ T_w=510 K we find $Dam_{het} \approx 10$, justifying the assumption $\omega_{v,w} \approx \omega_{v,eq}\{T_w; p\}$ in our preliminary PVTOS-ampoule simulations (Sections 3, 4).

As a corollary, this result implies:

$$\frac{\omega_{v,e}}{\omega_{v,w}} \approx \frac{\omega_{v,eq}\{T_e\}}{\omega_{v,eq}\{T_w\}} = \exp\left\{\mathcal{L}\left(1 - \frac{1}{\theta_e}\right)\right\} \qquad (2.4\text{-}7)$$

where:

$$\mathcal{L} \equiv \frac{\Lambda}{RT_w} \text{ (dimensionless heat of CuPc sublimation)} \qquad (2.4\text{-}8a)$$

and:

$$\theta_e \equiv \frac{T_e}{T_w} \text{ (temperature ratio)} \qquad (2.4\text{-}9)$$

Equation (2.4-4) further implies that for CuPc(s) sublimation, $\Lambda \approx 62.5$ K cal/mole, hence a typical value of $\mathcal{L}$ (@, say, 510 K) is quite large (cf. Section 4):

$$\mathcal{L} \equiv \frac{\Lambda}{RT_w} = \frac{62{,}500}{(1.987)(510)} = 62 \qquad (2.4\text{-}8b)$$

i.e., much larger than those (*ca.* 20) characterizing alkali sulfate deposition (see, *e.g.*, Castillo and Rosner, 1988; and Rosner *et al.*, 1979). This, when combined with Eq. 2.4-7, implies $\omega_{v,w} << \omega_{v,e}$ even at values of T_e/T_w only slightly greater than unity.

2.4.3 "Slip" (creep) along ampoule side walls

To the best of our knowledge, in all previous analyses of PVT and CVT in nonisothermal ampoules it has been explicitly or implicitly assumed that the motionless ampoule side walls bring any local gas *tangential* motion to rest — a condition known as the 'no-slip' condition. From this 'classical' perspective the side-walls 'damp' motions established as a result of gravity and/or Stefan flow (Section 2.4.1). However, we show below that, in fact, the nonisothermal side-walls can act like a 'pump' producing a side-wall gas 'creep' which would be present in the absence of gravity and/or Stefan flow! We conclude that this 'creep' phenomenon† will have to be included in all future PVTOS-transport modeling. Here we outline its essential features and show that vapor flows produced by side wall gas 'creep' are within one order-of-magnitude of vapor flows produced by gravity in ground-based laboratory PVTOS-experiments. In follow-on research, we will better define the nature of this side wall boundary condition and illustrate its dramatic effects for nonisothermal ampoules in the presence or absence of bouyancy-induced flows.

Over one century ago J.C. Maxwell pointed out that, unless gas/solid encounters were completely 'specular' (*i.e.* with no tangential momentum exchange) a nonuniform temperature

† This phenomenon is also the 'cause' of the so-called 'radiometer' motion (IR illuminated paddle-wheel in partial vacuum) as well as thermophoresis for poorly conductive particles in the near-continuum regime.

surface would induce a tangential motion (from cold to hot). For nearly 'diffuse' reflection from a locally adiabatic wall this velocity can be expressed (see, *e.g.*, Kennard, 1938) as:

$$v_{z,w} \cong 0.8\, v_{g,w} \cdot \frac{\partial \ln T_w}{\partial z} \qquad (2.4\text{-}10)$$

Its comparative importance can be appreciated by forming the Peclet group:

$$Pe_{creep} \equiv \frac{(v_{z,w})_{creep}\, L}{D_v} \approx \ln\left(\frac{T_e}{T_w}\right)^{0.8\ Sc} \approx 0.8\ Sc \cdot \frac{\Delta T}{T} \qquad (2.4\text{-}11)$$

Inserting, say, T_e/T_w=1.32 and Sc≈3.7 (Section 2.3) we find Pe_{creep}≈0.82, which, if it could prevail across the entire ampoule radius, would correspond to a CuPc(v) deposition rate reduction by the factor:

$$F(\text{thermal creep}) = \frac{Pe_{creep}}{\exp\{Pe_{creep}\} - 1} \approx 0.67 \qquad (2.4\text{-}12)$$

in the absence of complicating phenomenon (Soret effect, natural convection, ...). However, in practice, the upflow associated with thermal creep *along the nonisothermal ampoule side wall* will probably give rise to a core downflow, further contributing to the deposition rate augmentation associated with CuPc(v) Soret transport (Section 2.1). We expect those two effects to be non-negligible and "additive".

It is interesting to note that, in 1943, Kramers and Kistemaker pointed out that gas *composition* gradients can also contribute to gas mixture 'creep' along the solid surface. While they explicitly considered the simplest (binary isothermal gas) case, they showed that the slip would be directed toward the lighter gas. Recalling our discussion (Section 2.2) of Soret-induced separation in the H_2+Xe-containing carrier gas, this implies that the ampoule thermal gradient will cause a gas flow away from the film surface due to the 'direct' thermal creep, and the secondary (Soret-induced) 'composition creep'. Our preliminary estimates indicate this 'secondary' effect may also be quite important. However, more definitive conclusions will have to await follow-on research which generalizes the derivations of Maxwell, and Kramers & Kistemaker to nonisothermal gas mixtures of disparate molecular weight.

In considering the need for microgravity conditions, it is useful to compare the thermal creep velocity to the typical velocity: $(g\beta\Delta TL)^{1/2}$ resulting from bouyancy in a g-field. Using Eq. 2.4-10 and β=1/T, one finds:

$$\frac{(v_z)_{\text{thermal creep}}}{(v_z)_{\text{natural convection}}} \approx \frac{0.8\left(\frac{\Delta T}{T_w}\right)}{(Gr_h)^{\frac{1}{2}}} \qquad (2.4\text{-}13)$$

where Gr_h is the heat transfer Grashof number (Rosner, 1986):

$$Gr_h \equiv \frac{g\beta\Delta TL^3}{\nu^2} \qquad (2.4\text{-}14)$$

Inserting g=980 cm/s^2, β=1/T, L=7.5 cm for T_e=673 K and T_w=510 K, we find $Gr_h \approx 12$, and (from Eq. 2.4-13) a creep velocity which is about 6 percent of $(g\beta\Delta TL)^{1/2}$. This implies that *even in ground-based PVTOS-experiments one cannot neglect the thermal creep phenomenon.* In *microgravity* PVTOS experiments 'creep' is probably the dominant cause of vapor convection within the nonisothermal ampoule.

The importance of 'thermal creep' at the side-wall solid boundaries of this low density, strongly non-isothermal gaseous system also raises the interesting and rather fundamental question of the validity of the ordinary Newton-Stokes-Fourier 'closure' for the gas stresses and heat flux *within* this slow non-isothermal flow (SNIF). Indeed, Kogan (1973, 1986) has pointed out that, despite the smallness of the Knudsen number (here of order 10^{-3}) in such SNIFs, some of the Burnett terms (derived from the Boltzmann equation) which are dropped in traditional high Re, low Kn, low $\Delta T/T$ Navier-Stokes formulations (*i.e.*, Newton-Stokes-Fourier 'closure') are actually of the same order as the terms retained. While beyond the scope of the present pilot study, it now seems clear that future simulations should not only use 'creep boundary conditions' but also retain these so-called Burnett terms in the generalized constitutive laws governing the stresses and energy flux within the gas mixture. Kogan (1973, 1986) has shown that even in cases with perfectly isothermal non-symmetric walls of unequal temperature (*e.g.*, a 'corner') the Burnett terms lead to 'thermal stress convection'. In the PVTOS-ampoule situation with $\Delta T/T \approx 0.3$, we expect 'wall creep' to exceed 'thermal stress convection', but both effects will probably be important, especially under microgravity conditions.

2.4.4 Thermal boundary conditions

For purposes of the present preliminary study we have made the following simplifying assumptions regarding the important *thermal* boundary conditions for PVTOS in sealed cylindrical ampoules:

A1. The source temperature T_e and deposit surface T_w are radially uniform and specified.

A2. The side walls are nonisothermal but 'adiabatic' — *i.e.*, the site of negligible *radial* heat loss.

A3. The gas mixture at each of these surfaces has a temperature equal to that of the adjacent solid wall.

Regarding these assumptions, it should be commented that:

C1. more realistic temperature assignments, perhaps based, in part, on direct experiments (as employed by Miller, 1986) or finite-element heat conduction calculations for the actual PVTOS ampoule assemblies can be introduced in follow-on studies.

C2. In Section 3 we have examined the consequences (for natural convection) of relaxing the adiabatic side wall condition.

C3. The absence of appreciable temperature 'jump' phenomena (see, *e.g.*, A3, and Kennard, 1938) is associated with the combination of high *thermal* accommodation coefficient for buffer gas/side-wall encounters and small ampoule Knudsen numbers (l/d_w of order 10^{-3}).

2.5 Vapor Phase Supersaturations and Clustering

We show in Section 4.7 that when T_e/T_w is only about 1.32 and for values of $L \equiv \Lambda/RT_w$ of 62 convection-free CuPc(v) composition profiles calculated in the absence of mist formation (*i.e.*, "source-free" [sf] calculations) correspond to extremely large *local supersaturations* †† within the ampoule (near 10^5), and large values of the slope $(\partial s/\partial \eta)_{\partial v}$ (above 10^6) at the OS-film growth interface. Such conditions may have important implications for the growth of more highly ordered thin films, since:

E1. large vapor phase supersaturation would promote CuPc(v)-clustering (*i.e.* the formation of dimers, trimers, ...) which may complicate the process of crystal formation at the vapor/solid interface. Indeed, above some threshold ('critical' supersaturation) at high enough vapor densities, we would expect the formation of CuPc(s) "smoke" (Rosner and Epstein, 1968) — the collection of which would surely degrade film quality.

E2. Smooth surface growth may be impossible above a threshold value of $(\partial s/\partial \eta)_w$ because of "morphological instability" of the growing interface under such conditions (associated with the 'runaway' of asperities that reach into regions of higher local supersaturation).

Accordingly, in this program and our follow-on PVTOS research we will focus on the effects of gravity and microgravity conditions on the values of s_{max} and $(\partial s/\partial \eta)_w$ attained within the ampoule and at the OS-film surface, respectively. It seems likely that modest changes in the extent/nature of convection within the ampoule (see Section 3) will have important effects on s_{max} and $(\partial s/\partial \eta)_w$, which, in turn, will have dramatic effects on OS-film quality due to effects E1 and E2 above. Research to enable quantitative predictions of nucleation, clustering, and interface instability have been initiated but will be beyond the scope of this pilot study/report.

3. COMPUTATIONAL MODELING

3.1 Approach

In this section we describe a finite-difference code based on Newton's method for systems of nonlinear elliptic boundary value problems in two dimensions, and report results obtained from its application to steady axisymmetric laminar natural convection in a finite cylinder. Our implicit,

---

†† Defined here as $s \equiv \frac{p_v}{p_{v,eq}(T)}$ where $p_{v,eq}(T)$ is obtained from Eq. 2.4-4.

adaptive computational approach retains a degree of generality which is not fully necessary in the problems at hand but allows for subsequent incorporation of additional coupling effects with no significant alterations to code kernels. We have employed similar codes in one- and two-dimensional models of chemically reacting laminar flows, including detailed Arrhenius kinetics and detailed multi-component transport (Keyes and Smooke, 1987; Smooke *et al.*, 1987), and found them to be reliable in predicting internal energy and species distributions in comparison to experimental measurements (Puri *et al.*, 1987).

We begin with a presentation of the governing equations and boundary conditions, then describe the solution procedure and present some sample graphical results and key functionals of the converged solution, and conclude this section with a brief evaluation of the present and possible future states of the numerical modeling effort.

3.2 Governing Equations

Presuming axisymmetry and exploiting the near-isobaricity of the PVTOS test configuration under simulation, we adopt a Stream function-vorticity description of the flow field. Let r ($0 \le r \le R$) and z ($0 \le z \le L$) denote the radial and axial directions, v_r and v_z the respective velocity components, and ρ the density. We introduce the variable density Stokes Stream function ψ such that:

$$\rho\, r\, v_r = -\frac{\partial \psi}{\partial z} \quad \text{and} \quad \rho\, r\, v_z = \frac{\partial \psi}{\partial r},$$

and the (circumferential component of) vorticity Ω:

$$\Omega = \frac{\partial v_r}{\partial z} - \frac{\partial v_z}{\partial r},$$

along with its radially normalized form:

$$\Omega' = \frac{\Omega}{r},$$

The temperature is denoted T. The species concentrations by mass are denoted ω_j, for j=1, 2,..., J, where J is the number of species in the mixture. If one assumes Navier-Stokes-Fourier 'closure' (see Section 2.4.3), then these fields satisfy the following equations (see *e.g.*, Gosman *et al.*, 1969):

Stream function:

$$\frac{\partial}{\partial z}\left(\frac{1}{r\rho}\frac{\partial \psi}{\partial z}\right) + \frac{\partial}{\partial r}\left(\frac{1}{r\rho}\frac{\partial \psi}{\partial r}\right) + r\Omega' = 0. \qquad (3.2\text{-}1)$$

Normalized Vorticity:

$$r^2\left[\frac{\partial}{\partial z}\left(\Omega'\frac{\partial \psi}{\partial r}\right) - \frac{\partial}{\partial r}\left(\Omega'\frac{\partial \psi}{\partial z}\right)\right] - \frac{\partial}{\partial r}\left(r^3\frac{\partial}{\partial r}(\mu\Omega')\right) - \frac{\partial}{\partial z}\left(r^3\frac{\partial}{\partial z}(\mu\Omega')\right) + r^2 g\frac{\partial \rho}{\partial r} + r^2 \nabla\left(\frac{v_r^2 + v_z^2}{2}\right)\cdot \mathbf{iso}\ \rho = 0. \qquad (3.2\text{-}2)$$

Internal Energy:

$$c_p\left[\frac{\partial}{\partial z}\left(T\frac{\partial\psi}{\partial r}\right)-\frac{\partial}{\partial r}\left(T\frac{\partial\psi}{\partial z}\right)\right]-\frac{\partial}{\partial r}\left(rk_h\frac{\partial T}{\partial r}\right)-\frac{\partial}{\partial z}\left(rk_h\frac{\partial T}{\partial z}\right)$$
$$+r\sum_{j=1}^{J}\left[\rho\, c_{pj}\,\omega_j\left(V_{j_r}\frac{\partial T}{\partial r}+V_{j_z}\frac{\partial T}{\partial z}\right)\right]+r\sum_{j=1}^{J}h_j M_j \dot{r}_j'''=0. \qquad (3.2\text{-}3)$$

Species Mass Fraction:

$$\frac{\partial}{\partial z}\left(\omega_j\frac{\partial\psi}{\partial r}\right)-\frac{\partial}{\partial r}\left(\omega_j\frac{\partial\psi}{\partial z}\right)+\frac{\partial}{\partial r}(r\,\rho\,\omega_j\,V_{j_r})+\frac{\partial}{\partial z}(r\,\rho\,\omega_j\,V_{j_z})$$
$$-r\,M_j\,\dot{r}_j'''=0,\quad j=1,2,\ldots,J. \qquad (3.2\text{-}4)$$

Other parameters appearing in this system are: the mixture viscosity μ, the acceleration of gravity g, the diffusion velocities of the j^{th} species in the mixture (V_{jr}, V_{jz}), the specific heat of the j^{th} species c_{pj}, the specific heat of the mixture c_p, the thermal conductivity of the mixture k_h, the molecular mass of the j^{th} species M_j, and the generation/consumption rate of the j^{th} species due to chemical reaction, if any, $\dot{r}_j'''$.

The system is closed with the multicomponent ideal gas law,

$$\rho=\frac{p\,\overline{M}}{RT},$$

where $\overline{M}$ is the mixture molecular mass and p is the pressure. Thermodynamic and constitutive equations provide the temperature- and composition-dependent specific heats, viscosities, thermal conductivities, and diffusion velocities. A chemical kinetics model would provide the $\dot{r}_j'''$ if necessary (for CVD simulations).

For present purposes, we shall assume no homogeneous chemical reaction, which allows dropping the $\dot{r}_j'''$ terms. As additional simplifications, we shall distinguish between the CuPc vapor and carrier gases only, assuming that the carrier gas may be characterized as a homogeneous mixture, and furthermore that the vapor is present in the trace limit. Under this pair of assumptions, overall mass conservation is enforced by the continuity equation, and it is necessary to consider only one species equation (J=1), that for the vapor itself. In the vapor species equation, the diffusion velocities may be replaced by Fickian and Soret terms involving only vapor and temperature gradients. The characterization of the carrier gas with a composition-independent specific heat enables dropping the term containing diffusion velocities in the energy equation. The latter two equations then possess the forms:

Temperature:

$$c_p\left[\frac{\partial}{\partial z}\left(T\frac{\partial\psi}{\partial r}\right)-\frac{\partial}{\partial r}\left(T\frac{\partial\psi}{\partial z}\right)\right]-\frac{\partial}{\partial r}\left(r\,k_h\frac{\partial T}{\partial r}\right)-\frac{\partial}{\partial z}\left(r\,k_h\frac{\partial T}{\partial z}\right)=0. \qquad (3.2\text{-}5)$$

Vapor Mass Concentration:

$$\frac{\partial}{\partial z}\left(\omega_v \frac{\partial \psi}{\partial r}\right) - \frac{\partial}{\partial r}\left(\omega_v \frac{\partial \psi}{\partial z}\right)$$
$$- \frac{\partial}{\partial r}\left(r \rho D_v \left[\frac{\partial \omega_v}{\partial r} + \alpha_T \frac{\omega_v}{T}\frac{\partial T}{\partial r}\right]\right) - \frac{\partial}{\partial z}\left(r \rho D_v \left[\frac{\partial \omega_v}{\partial z} + \alpha_T \frac{\omega_v}{T}\frac{\partial T}{\partial z}\right]\right) = 0. \qquad (3.2\text{-}6)$$

The subscript j has been dropped, and α_T is the Soret coefficient for the vapor in the mixture. The transport coefficients retain their temperature dependence.

3.3 Boundary Conditions

The geometry of the cylinder requires posing three types of boundary conditions: symmetry conditions at r=0, end-wall conditions at z=0 and z=L, and lateral conditions at r=R. Equations (3.2-1)-(3.2-2) and (3.2-6)-(3.2-5) comprise an elliptic set and require four conditions (on the values or gradients of the principal fields) at each boundary point. These are presented below, grouped by boundary type.

3.3.1 Symmetry Boundaries

On a symmetry boundary, the fields satisfy zero-normal gradient conditions. In addition, the velocity normal to the symmetry boundary must be zero by continuity. This implies that the Stream function will be a constant along the boundary. We choose this constant to be zero along the axis of symmetry. The vorticity is also zero there, from the requirements that $v_r=0$ and $(\partial v_z)/\partial r=0$. However, the normalized vorticity $\Omega' \equiv \Omega/r$ is not necessarily zero, since its denominator also vanishes to first order. We derive a condition on Ω' from the local expansion of the stream-function:

$$\psi(z) = a_2(z)r^2 + a_4(z)r^4 + \ldots .$$

Together with the identity

$$\Omega = -\frac{\partial}{\partial z}\left[\left(\frac{1}{\rho r}\right)\frac{\partial}{\partial z}\psi\right] - \frac{\partial}{\partial r}\left[\left(\frac{1}{\rho r}\right)\frac{\partial}{\partial r}\psi\right]$$

and the constancy of ψ along the axis, this implies that $\Omega \approx -8a_4 r/\rho$. (In the practical encoding of this boundary condition, a_4 may be evaluated by differencing radially adjacent values of ψ)
We therefore have, for r=0, $0 \le z \le L$:

Stream function:

$$\psi = 0.$$

Normalized Vorticity:

$$\Omega' \approx -\frac{8a_4}{\rho}.$$

Temperature:

$$\frac{\partial T}{\partial r} = 0.$$

Vapor:

$$\frac{\partial \omega_v}{\partial r} = 0.$$

3.3.2 End-wall Boundaries

The end-wall boundary conditions depend upon whether Stefan flow is incorporated. In this treatment, Stefan flow is neglected; thus, $v_z(r,z)=0$ at z=0 and z=L. Combined with the fact that the end-walls are no-slip surfaces, this implies that $\psi = 0$, as on the axis. The vorticity at the wall may be specified in terms of the Stream function derivatives, as in (3.2-1). In encoding this boundary condition, radial terms vanish, and the axial terms of (3.2-1) can be evaluated by second differences of ψ. (The term proportional to $\partial\psi/\partial z$ vanishes by the no-slip condition on v_r). We shall assume that end-wall temperatures are fixed by contact with thermal reservoirs, and hence that temperature satisfies a Dirichlet constraint. Similarly, we assume Dirichlet conditions on vapor mass fraction, based on an equilibrium model.

We therefore have, for $0 \le r \le R$:

Stream function:

$$\psi = 0.$$

Normalized Vorticity:

$$\Omega' = -\frac{1}{r^2 \rho}\frac{\partial^2 \psi}{\partial z^2}$$

Temperature:

$$T = T_e \quad \text{or } T = T_w.$$

Vapor:

$$\omega_v = \omega_{v,eq}\{T_e;p\} \quad \text{or } \omega_v = \omega_{v,eq}\{T_w;p\}$$

3.3.3 Lateral Boundaries

The lateral boundary conditions depend upon whether assumptions of no creep, thermal adiabaticity, and non-absorbing vapor-wall collisions are made. One of the principal uses of future computer modeling in the PVTOS context will, in fact, be evaluating the sensitivity of the flow to lateral boundary treatments. Under any of these assumptions, we may assume no-flux boundary conditions for the dilute mixture, so that ψ is handled as above. The possibility of creep is retained in the lateral wall model by not forcing the term in $\partial\psi/\partial r$ to vanish but retaining it in a derivation of Ω' through (3.2-1). The main alternatives for the vapor are local equilibrium (non-homogeneous Dirichlet) or non-absorbing (homogeneous Neumann). The temperature boundary condition is modeled along a continuum from Dirichlet to Neumann. The heat flux $k_h(\partial T/\partial r)$ at r=R is assumed proportional through a film coefficient h to a difference between the temperature itself and an

ambient external temperature representing a reservoir beyond an imperfectly insulating wall. Taking h=0 corresponds to adiabaticity. Mathematically, we can summarize as follows, for r=R, $0 \le z \le L$:

Stream function:

$$\psi = 0.$$

Normalized Vorticity (no-slip or creep):

$$\Omega' = -\frac{1}{r^2\rho}\frac{\partial^2\psi}{\partial r^2} \quad \text{or} \quad \Omega' = -\frac{1}{r}\frac{\partial}{\partial r}\left(\frac{1}{r\rho}\right)\frac{\partial\psi}{\partial r} - \frac{1}{r^2\rho}\frac{\partial^2\psi}{\partial r^2}.$$

Temperature:

$$\frac{\partial T}{\partial r} = \frac{h}{k_h}(T - T_{amb}).$$

Vapor (equilibrium or non-absorbing):

$$\omega_v = \omega_{v,eq}(T;p) \quad \text{or} \quad \frac{\partial \omega_v}{\partial r} = 0.$$

where, for the case of thermal creep, $(\partial\psi/\partial r)$ is evaluated using Eq.(2.4-10)

3.4 Parameterization

In this subsection we further specialize the governing equations and boundary conditions to detail the parameters used in the reported numerical simulations. In anticipation of incorporating the CGS-based subroutine package CHEMKIN (Kee *et al.*, 1980, 1983) in future treatments of the multicomponent case, the equations are encoded in the *dimensional* forms shown above. To display the common structure of these equations we rewrite them in tabular form below. Each of the equations can be written in the generic convection-diffusion form:

$$a\left[\frac{\partial}{\partial z}\left(\phi\frac{\partial\psi}{\partial r}\right) - \frac{\partial}{\partial r}\left(\phi\frac{\partial\psi}{\partial z}\right)\right] - \frac{\partial}{\partial z}\left[(br)\frac{\partial}{\partial z}(c\phi)\right] - \frac{\partial}{\partial r}\left[(br)\frac{\partial}{\partial r}(c\phi)\right] - rd = 0 \qquad (3.4\text{-}1)$$

where ϕ takes on the meaning of each of the four fields in combination with the coefficients:

Table 3.4-1

Summary of the governing partial differential equations in terms of the generic equation (3.4-1)

ϕ	a	b	c	d
ψ	0	$1/(r^2\rho)$	1	Ω'
Ω'	r^2	r^2	μ	s_Ω
T	c_p	k_h	1	0
ω_v	1	ρD_v	1	s_ω

and the vorticity and vapor "source" terms:

$$s_\Omega = -r\left\{g\frac{\partial\rho}{\partial r} + \frac{1}{2}\left[\frac{\partial}{\partial r}\left(v_r^2 + v_z^2\right)\cdot\frac{\partial\rho}{\partial z} - \frac{\partial}{\partial z}\left(v_r^2 + v_z^2\right)\frac{\partial\rho}{\partial r}\right]\right\},$$

$$s_\omega = \frac{\partial}{\partial r}\left(r\,\rho\,D_v + \alpha_T\frac{\omega_v}{T}\frac{\partial T}{\partial r}\right) + \frac{\partial}{\partial z}\left(r\,\rho\,D_v + \alpha_T\frac{\omega_v}{T}\frac{\partial T}{\partial z}\right).$$

The temperature- and pressure-dependence of the properties are defined with respect to a reference state at p_0=3.2 Torr =4.21x10^{-3} atm and T_0=600 K, with a reference density of ρ_0=3.18x10^{-6} g cm^{-3}, as determined from the ideal gas law with $\overline{M}$=37.2. This pressure is the nominal operating pressure for the PVTOS ampoule, and the temperature is conveniently mid-range. The transport and thermodynamic properties are:

$$\mu = 3.05\times10^{-4}\,(T/T_0)^{0.778}\ \text{g cm}^{-1}\,\text{s}^{-1},$$

$$k_h = 1.86\times10^{-4}\,(T/T_0)^{0.665}\ \text{cal cm}^{-1}\,\text{s}^{-1}\,\text{K}^{-1},$$

$$D_v = 29.1\,(T/T_0)^{3/2}\,(p_0/p)\ \text{cm}^2\,\text{s}^{-1},$$

$$\alpha_T = 2.33\,(T/T_0)^{0.278},$$

$$c_p = 0.226\,(T/T_0)^{0.177}\ \text{cal g}^{-1}\,\text{K}^{-1}.$$

The parameters required in the posing of the boundary conditions are, *e.g.*:

$$T_w = 510\ \text{K},$$
$$T_e = 673\ \text{K},$$

along with the equilibrium vapor pressure law (2.4-4) which translates into an equilibrium mass fraction by means of the formula

$$\omega_v = \frac{M_v}{\overline{M}}\frac{p_v}{p_0}.$$

3.5 Discretization Procedure

The governing equations, along with appropriate boundary conditions, are differenced on a two-dimensional tensor product grid which is generated adaptively from an initial coarse grid by

subequidistribution of gradients and curvatures of the solution components. This concentrates gridpoints in the regions of high-activity (fronts and peaks) in the domain. Second-order differences are used throughout except for gradient boundary conditions and for the convective terms of the vorticity, energy and species equations, in which first-order upwind differences are employed. This discretization can be accommodated within the standard nine-point stencil, and the diagonal dominance of the Jacobian, a key consideration in the implicit numerical solution of the Newton correction equations, is thereby insured.

Ordering the solution components at each gridpoint most rapidly, followed by a natural ordering of the gridpoints themselves (radial index varying more rapidly than axial index), results in a Jacobian which has a standard block nine-diagonal structure. To solve this system, we employ a block relaxation method in which only the diagonal blocks are factored by a direct method, and the six blocks in the wings of the Jacobian are thrown to the right-hand side. As the outermost loop in the relaxation process used to solve the linear problems at each Newton step, the domain is swept repeatedly in the axial direction from upstream to downstream. This takes advantage of the high aspect ratio of domain, which makes the coefficients arising from the radial diffusion terms numerically dominant.

The complexity of the governing equations precludes convenient analytic expression of the elements of the Jacobian; therefore a finite-difference approximation to the Jacobian must be used. Extending the ideas of Curtis *et al.* (1974) we can form all of the nonzero elements from 9x4+1=37 independent vector residual evaluations (with the 9 arising from the number of points in the finite difference stencil, and the 4 from the number of independent fields).

3.6 Solution Procedure

We consider in this section a discretized elliptic system in the generic form

$$F(\phi) = 0 \tag{3.6-1}$$

where ϕ is a vector of unknowns, and F is a vector-valued function with the same number of components as ϕ in which ϕ may enter nonlinearly.

The system Eq. (3.6-1) may be solved efficiently for ϕ by a damped modified Newton method provided that an initial iterate $\phi^{(0)}$ sufficiently close to the solution ϕ^* is supplied. The damped modified Newton iteration is given by

$$\phi^{(k+1)} = \phi^{(k)} + \lambda^{(k)} \delta\phi^{(k)} \tag{3.6-2}$$

where

$$\delta\phi^{(k)} = -\left(\tilde{J}^{(k)}\right)^{-1} F\left(\phi^{(k)}\right), \tag{3.6-3}$$

where the matrix $\tilde{J}^{(k)}$ is an approximation to the actual Jacobian matrix evaluated at the k^{th} iterate. We refer to $\delta\phi^{(k)}$ as the k^{th} update. When

$$\lambda^{(k)} = 1 \text{ and } \tilde{J}^{(k)} = J^{(k)} \equiv \frac{\partial F}{\partial \phi}\left(\phi^{(k)}\right),$$

for all k, a pure Newton method is obtained.

For the pure Newton method, the iteration of Eq. (3.6-2) and Eq. (3.6-3) possesses at least a quadratic rate of convergence asymptotically. Mathematically, this implies that that is, $\|\phi^{(k+1)} - \phi^*\| \le c\|\phi^{(k)} - \phi^*\|^2$ for some constant c, so that the number of significant figures of accuracy doubles at each iteration, asymptotically. (Rates of convergence close to this are obtained in practice.) For the modified Newton method without restarting (*i.e.*, with $\tilde{J}^{(k)} = \partial F/\partial\phi\left(\phi^{(0)}\right)$ for all $k \ge 0$) the rate of convergence is not guaranteed to be better than linear, and the number of significant figures of accuracy may improve asymptotically at only a constant rate. Consequently, there is a tradeoff to be made between the higher cost per iteration of the pure Newton method and the higher iteration count of a modified Newton method. We resolve this tradeoff by reevaluating the Jacobian at irregular intervals which are dictated adaptively by the progress of the iterations.

A better initial condition for Newton's method is usually obtainable by an elementary continuation procedure, namely driving a pseudo-transient form of Eq. (3.6-1),

$$D\frac{\partial \phi}{\partial t} + F(\phi) = 0 \qquad (3.6\text{-}4)$$

where D is a scaling matrix, part of the way towards its steady state until the domain of convergence of Newton's method is reached. If Eq. (3.6-4) is implicitly time-differenced with the backward Euler method, using time step Δt from a given initial state $\bar{\phi}$ a new system,

$$\bar{F}(\phi) \equiv D\frac{(\phi - \bar{\phi})}{\Delta t} + F(\phi) = 0 \qquad (3.6\text{-}5)$$

results, which possesses the Jacobian

$$\bar{J} \equiv \frac{D}{\Delta t} + \frac{\partial F}{\partial \phi}.$$

For a succession of time steps, Δt, which will in general be coarser than what would be required for accurate resolution of the physical transient, the iteration of Eq. (3.6-5) is a numerically robust procedure for generating an initial iterate for Newton's method. Moreover, due to the close relationship of Eq. (3.6-5) to Eq. (3.6-1), only minor modifications of the steady-state code for Eq. (3.6-1) are required to make it a transient/steady-state hybrid. Adaptive control of the size of the time steps used in Eq. (3.6-5) can enhance the efficiency of such a hybrid algorithm. A useful strategy which we employ in the current code is to choose Δt based on the temporal truncation error of the most rapidly varying component of the solution. As ϕ approaches ϕ^* and Δt becomes large, this effects a smooth transition to the (infinite time step) steady-state formulation. We emphasize that although the current code has transient analysis capabilities, it will ordinarily be

too computing intensive to use this capability on anything but supercomputers, and no transient diagnostics have been assembled for it.

Insertion of the Burnett terms referred to in Section 2.4.3 is formally straightforward as a future modification. The viscous, mass, and thermal fluxes receive additional contributions. Some of the terms force an expansion of the finite difference stencil; beyond nine points they may be retained in the governing equations in $F\{\phi\}$. The Jacobian then becomes only approximate, but should still serve as a useful means of advancing the convergence of the solution through (3.6-2)-(3.6-3)

3.7 Illustrative Results

We present in this subsection illustrative numerical modeling results for four problems: (1) a simulation of the CuPc cell under representative operating conditions with the adiabatic, non-absorbing set of boundary conditions conventionally assumed, (2) a simulation of the same cell with parasitic heat loss boundary conditions, (3) a simulation of the same cell with parasitic heat loss boundary conditions and equilibrium sidewall vapor boundary conditions, and (4) a simulation of a cell at much higher pressure. The runs with lateral wall boundary conditions other than the "standard" set are included in order to illustrate behaviors without the development of free convective cells that dramatically affect deposition region supersaturations, yet which may not be consciously controlled in current crystal growth practice. The reason for including higher pressure simulation is that the low Rayleigh numbers characteristic of standard operating conditions preclude the formation of the natural convection cell which has at times been presumed to be the key distinguishing feature between successful crystal growth in microgravity and less successful growth at ±1 g. Crudely speaking, the Rayleigh number is a dimensionless ratio of gravitational forcing due to density gradients to viscous and thermal dissipation, which for our purposes may be written as

$$Ra = \frac{g\left(\frac{\Delta \rho}{\rho_{ref}}\right) L^3}{\alpha_{ref} \nu_{ref}} .$$

The minimum Rayleigh number required for the onset of axisymmetric natural convection with adiabatic sidewalls depends on ampoule aspect ratio, and as will be shown below, is much larger than is met at standard operating conditions for an aspect ratio of height to radius of 10.

3.7.1 The "Standard" Cell

We display solutions for the standard operating conditions in an aspect ratio 10 ampoule in Fig. 3.7-1. A 21x47 grid covering half of a symmetry plane is shown. The origin is in the lower left corner, with the upper right at (R,L). The Rayleigh number is 4.76. The gravity vector points

upward but at such low Ra this is immaterial. Because of the absence of convection, $\psi=\Omega'=0$ to machine precision, and we present just the temperature contours (from 510 K at the base to 673 K at the top, in equi-increments of 10 K) and the CuPc mass concentration contours (from the equilibrium value of 1.24×10^{-9} at the base to 3.82×10^{-3} at the top, in equi-increments of 10^{-4}). The combination of no convection and adiabatic lateral conditions renders the flow field entirely one-dimensional. The key functionals obtained from the numerical results desired for comparison with the analytic results of section 4 are: the Nusselt numbers for mass and heat transfer evaluated at the deposition wall, the peak supersaturation value of ω_v along the centerline (and its ordinate), and the dimensionless supersaturation gradient at the wall. Labeling these quantities as in section 4, we find $Nu_m=1.44$, $Nu_h=1.10$, $s_{max}=7.5\times10^4$ at $z_{max}=.32$ cm, and $\partial s/\partial\eta|_{z=w} = 4.4\times10^6$.

3.7.2 The "Standard" Cell with Parasitic Lateral Heat Loss

We next consider standard operating conditions except for heat loss to an ambient reservoir maintained at the cold boundary temperature through only partially insulated side walls. Corresponding to increasingly greater heat loss, we have considered a succession of coefficients *h* in

$$\frac{\partial T}{\partial r} = \frac{h}{k_h}(T-T_{amb})$$

such that $h/k_h=c/R$ for c=1,10,100. A result for $h/k_h=100/R$ is shown in Fig. 3.7-2. The contour plots are drawn as before, and we have $Nu_m=0.325$, $Nu_h\approx0$, $s_{max}=1.7\times10^6$ at $z_{max}=5.6$ cm, and $\partial s/\partial\eta|_{z=w} = 1.0\times10^6$. The ≈0 notation means that the computed result is less than the square-root of the machine double precision for the microVAX, namely on the order of 10^{-8}, and therefore bears no significant figures. Almost all of the heat which enters from the top leaves from the lateral walls.

3.7.3 Combined Parasitic Lateral Heat Loss and Vapor Equilibrium

As a further illustration of the effect of lateral boundary conditions on the supersaturation gradient at the deposition surface, we consider again the previous problem with a different assumption on ω_v at the lateral boundary, namely that it is in thermal equilibrium with the wall temperature. The contour plots are drawn as before, and we have $Nu_m=0.00116$, $Nu_h\approx0$, $s_{max}=7.3\times10^4$ at $z_{max}=6.4$ cm, and $\partial s/\partial\eta|_{z=w} = 8.2\times10^3$.

3.7.4 A Convective Example

Through the definitions of the thermal and momentum diffusivities in terms of the density, and through the ideal gas law, the pressure enters the Rayleigh number invisibly to the second power. A thousand-fold increase in pressure results in a million-fold increase in Ra. With

increasing background pressure, the system moves into a region of parameter space where convection sets in.

An axisymmetric numerical solution in the convective case may or may not be physically realizable, due to instability with respect to nonaxisymmetric perturbations, as might occur, for instance, in actual lateral boundary conditions. Nevertheless, as an illustration of the full nonlinear capabilities of the code, we present one such case in Fig. 3.7-4. The five plots show, respectively, an adaptively refined 12x31 grid, the Stream function (positive, hence indicating a clockwise flow), the vorticity, the temperature, and the vapor mass fraction. The vapor mass fraction is more strongly influenced than the temperature by the convection since the Lewis number ($Le=D_v/\alpha_h$) is approximately 0.11 for this problem. The fact that the internal energy equation is more diffusively dominant than the vapor mass fraction equation is evidenced by temperature contours more nearly parallel to the purely diffusive case of Fig. 3.7-1. Though purely of academic interest because of its unrealizability, the maximum supersaturation along the center axis occurs very close to the deposition surface in this case ($z_{max}=0.072$ cm) and is significantly greater than encountered above ($s_{max}=3.9x10^7$), making the supersaturation gradient enormous ($8.6x10^9$).

3.8 Discussion

The sampling of solutions presented above shows that the presence or the absence of bouyancy-induced convection is neither necessary in accounting for large differences in the deposition wall environment of the CuPc ampoule, nor is it even the most likely cause of such differences. Rather lateral boundary condition non-uniformities or non-idealities have been pinpointed as potentially significant effects. Between the cases of Sections 3.7.1 and 3.7.3, a factor of 1000 reduction in Nu_m and of 500 in supersaturation gradient along the axis of symmetry is observed, simply by scavenging heat or heat and mass from the sidewalls in non-convective configurations. Indeed, in the aspect ratio under consideration the lateral boundary area of 35.3 cm^2 is twenty times greater than that of the deposition surface, and almost all of it is geometrically closer to the source of the vapor than is the deposition surface. It is natural to expect that proper manipulation of the sidewall temperature distribution will be a key engineering challenge to successful crystal growth. This should be easier to achieve in terrestrial applications than in orbit. In recognition of the importance of the thermal conditions at the lateral wall, Catton (1972) has coined the term "wall admittance" for the dimensionless number Lk_h/d_wk_w where d_w and k_w are the thickness and the thermal conductivity of the wall itself, whose control is analogous to our control of h in Section 3.7.

What is known experimentally and theoretically about natural convection in cylinders of aspect ratio 10 supports the basic conclusion drawn from the simulations presented above, namely that convection is unimportant until much higher Rayleigh numbers. Müller and Neuman (1983)

find that for a cylindrical cavity heated uniformly from below natural convection begins at a critical Rayleigh number (Ra_{cr}) of approximately 1.0×10^6. The onset varies with the lateral wall boundary conditions on the temperature. With perfectly conducting walls (which would establish a linear temperature gradient between the upper and lower surfaces), the onset is delayed until approximately 2.4×10^6. Perfectly insulating walls reduce the threshold to approximately 8.0×10^5. Their experimentally observed transition points agree well with the theoretical results of Charlson and Sani (1971).

The first experimentally accessible convective cell beyond this critical Rayleigh number is three-dimensional and non-axisymmetric. It is *not* the toroidal flow pattern computed in Section 3.4.7 by imposing axisymmetry; rather the flow rises along half of the lateral wall and falls along the other half. This single steady cell divides into three separate cells at approximately 2.5 Ra_c, then becomes unsteady at about 5.7 Ra_c, and eventually returns to a steady convoluted cell at approximately $Ra = 10^7$. (All of these higher bifurcation points in Ra also depend upon the sidewall conditions. For better-insulating sidewalls (plexiglass) the numbers decrease; for better-conducting sidewalls (aluminum), they increase.) Above 1×10^7, hysteresis affects the branch selection, depending upon whether the temperature differential is increasing or decreasing, and further unsteady behaviors of different types are observed. All behaviors above the non-convective one are beyond the reach of a two-dimensional simulation. Fortunately, a three-dimensional fluid dynamical model may not be necessary in future investigations, since the only flows which may be significant at standard operating conditions are those of the thermal creep variety.

4. PARAMETRIC STUDIES via ONE-DIMENSIONAL 'DIFFUSION-LIMIT' EXACT SOLUTIONS

4.1 Tractable Limiting Case: Simplifications

Considerable insight can be obtained readily in the 'convectionless' one-dimensional case, by including the effects of Soret transport and variable background gas thermophysical properties. While it may be argued that this case is overly idealized (neglecting the effects of bouyancy-induced convection [Section 3], side wall 'creep'-induced convection [Section 2.4.3], Stefan flow [Section 2.4.1], and side wall losses of heat and vapor mass [Section 2.4.4]), the facts that it leads to closed-form expressions and allows economical parametric studies, as well as asymptotic checks on more comprehensive numerical schemes (Section 3) more than justifies its inclusion and use here. In particular, we employ these asymptotic solutions to examine in the 'convectionless' cases, the nature of vapor concentration and temperature *profiles* within the ampoule (Section 4.4) and, hence, the associated local vapor supersaturations within the ampoule and in the immediate vicinity

of the OS-film surface (Section 4.7). Our closed-form results facilitate parametric studies (*e.g.*, of the effect of Soret coefficient α_T and ampoule temperature ratio T_e/T_w on OS-film growth rates, heat transfer rates and supersaturations. They also reveal most of the relevant dimensionless groups (Section 4.3) and their effects, thereby reducing the burden of examining all cases of potential interest in the presence of, say, natural convection (Section 3). Of course, we exploit the simplifications shown in Sections 2.2, 2.4.1, 2.4.2, to be reasonable under typical PVTOS-conditions; viz, negligible Soret separation in the background gas, negligible Stefan flow, and local vapor/solid equilibrium at stations ⓔ and ⓦ . However, we explicitly include the significant role of α_T-values of potential PVTOS interest (2-10), and we implicitly allow the molecular diffusivities D_v and $k/(\rho c_p)$ to differ (both in magnitude** and temperature dependence).

4.2 Equations Governing the 'Diffusion' Limit

Subject to the assumptions described in Section 4.1 the one-dimensional 'diffusion' limit is governed by the steady-state *energy* balance condition:

$$-\dot{q}''_z = k\{T\} \cdot \frac{dT}{dz} = \text{const.} = -\dot{q}''_w \qquad (4.2\text{-}1)$$

and the dilute vapor species balance condition:

$$-\dot{j}''_v = D_v \rho \left[\frac{d\omega_v}{dz} + \alpha_T \omega_v \frac{d \ln T}{dz}\right] = \text{const.} = -\dot{j}''_{v,w} \qquad (4.2\text{-}2)$$

(the momentum balance condition degenerates to p = const.).

If the indicated coefficients have the following 'power law' behavior:

$$k = k\{T_w\} \cdot \left(\frac{T}{T_w}\right)^{\varepsilon} \qquad (4.2\text{-}3a)$$

$$\rho = \rho\{T_w;p\} \cdot \left(\frac{T}{T_w}\right)^{-1} \qquad (4.2\text{-}3b)$$

$$D_v = D_v\{T_w;p\} \cdot \left(\frac{T}{T_w}\right)^{n} \qquad (4.2\text{-}3c)$$

$$\alpha_T = \text{const.} \qquad (4.2\text{-}3d)$$

then we can readily find the corresponding steady-state profiles of T and ω_v within the ampoule, as well as the wall fluxes $-\dot{q}''_w$ and $-\dot{j}''_{v,w}$, subject to the imposed 2-point boundary conditions:

$$T\{0\} = T_w(\text{spec.}),\ T\{L\} = T_e(\text{spec.}) \qquad (4.2\text{-}4a,b)$$

$$\omega_{v,w} = \omega_{v,eq}\{T_w;p\} \text{ (see Section 2.4.2)} \qquad (4.2\text{-}4c)$$

$$\omega_{v,e} = \omega_{v,eq}\{T_e;p\} \text{ (see Section 2.4.2)} \qquad (4.2\text{-}4d)$$

where $\omega_v \equiv \frac{\rho_v}{\rho} = \frac{p_v M_v}{\rho RT}$, $p_{v,eq}\{T\}$ is governed by Eq. 2.4-4, and $\rho = \frac{pM_g}{RT}$ where M_g is the mean molecular weight of the background "perfect" gas, here assumed constant (cf. Section 2.2).

** It will be seen that only $D_v(T;p)$ and $k\{T\}$ enter the present steady-state 'convectionless' calculations, not the thermal diffusivity α_{th}.

Once the ω_v and T-profiles are available (versus $(\eta \equiv z/L)$) it is straightforward to calculate the local "supersaturation" (Section 2.5)

$$s \equiv \frac{p_v}{p_{v,eq}(T)} = \frac{\omega_v}{\omega_{v,eq}(T)} \qquad (4.2\text{-}5)$$

and, hence, its derivative (ds/dz) evaluated at z=0.

4.3 Relevant Dimensionless Groups

Inspection of the equations/boundary conditions (ODEs/BCs) of Section 4.2 reveals that, once the relevant property variation exponents $d(\ln k)/d(\ln T)\equiv\varepsilon$ and $d(\ln D_v)/d(\ln T)\equiv n$ are selected, all dimensionless dependent variables will be functions of only the three important parameters: $T_c/T_w\equiv\theta_e$, $\mathcal{L}\equiv\Lambda/(RT_w)$ and the (assumed constant) Soret factor α_T. The dependent quantities of greatest interest are s_{max}, $(ds/d\eta)_w$, and two (dimensionless) wall fluxes:

$$Nu_m \equiv \frac{-j''_{v,w}}{\left\{\frac{(D_v\rho)_w(\omega_e-\omega_w)}{L}\right\}} \equiv \text{Nusselt number for } \textit{mass} \text{ transfer through gas} \qquad (4.3\text{-}1)$$

$$Nu_h \equiv \frac{-q''_w}{\left\{k_w\frac{(T_e-T_w)}{L}\right\}} \equiv \text{Nusselt number for zz } \textit{heat} \text{ transfer through gas} \qquad (4.3\text{-}2)$$

In the illustrative calculations displayed below we have selected the representative property-value exponents $\varepsilon=2/3$, $n=3/2$, and allowed θ_e,$\mathcal{L}$ and α_T to take on values relevant to a variety of PVTOS situations, *viz.* $1\le\theta_e\le2$, $\mathcal{L}=10(20)90$ (*i.e.*, 10 through 90 with intervals of 20), $\alpha_T=0(2)10$. It will be appreciated that these "cases" actually cover a wide variety of thermophysical situations in terms of actual absolute temperatures, ampoule pressures, source vapor identity, background gas identity, etc. Indeed, if absolute fluxes of heat and/or mass to the gas-film surface are needed one must supplement the displayed Nu_m, Nu_h-values (Eq. 4.3-1, 4.3-2) by the relevant absolute values of the (bracketed) reference fluxes' (see, *e.g.*, Rosner, 1986). Apart from the graphs included later in this section, it is easy to use the explicit closed-form relations provided below to calculate the quantities of interest for *any* new combination of the parameters: θ_e, L, α_T; ε, n.

4.4 Fields of Mixture Temperature and Vapor Concentrations

Integration of the energy balance condition (4.2-1) subject to BC (4.2-4a,b) leads to the following simple (inverted) expression for the temperature ratio $\theta\equiv T/T_w$ at each $z/L\equiv\eta$.

$$\eta = \frac{\theta^{1+\varepsilon}-1}{\theta_e^{1+\varepsilon}-1} \qquad (4.4\text{-}1)$$

showing that the temperature profile is not linear when $\varepsilon\neq0$ (temperature-dependent thermal conductivity). It is convenient to suppress z/L and treat the vapor mass balance equation using

local temperature as an independent variable. One is then led to a readily integrable first order linear homogeneous ODE for $d\omega_v/d\theta$, with the explicit result:

$$\frac{\omega_v}{\omega_{v,eq}(T_w)} = \frac{\theta^{-\alpha_T}}{\theta_e^{\beta}-1}\cdot\left[\theta^{\beta} - \frac{\theta_e^{\alpha_T} - \theta_e^{\beta}\exp\left(-\mathcal{L}\left(1-\frac{1}{\theta_e}\right)\right)}{\theta_e^{\alpha_T} - \exp\left(\mathcal{L}\left(1-\frac{1}{\theta_e}\right)\right)}\right] \times\left[\frac{\theta_e^{\alpha_T} - \exp\left(-\mathcal{L}\left(1-\frac{1}{\theta_e}\right)\right)}{\exp\left(-\mathcal{L}\left(1-\frac{1}{\theta_e}\right)\right)}\right] \qquad (4.4\text{-}2)$$

where we have introduced the composite exponent:

$$\beta = \alpha_T + \varepsilon + (2-n) \qquad (4.4\text{-}3)$$

a typical value of which is: $\beta = 2 + \frac{2}{3} + \left(2-\frac{3}{2}\right) = 3.16$

These closed-form expressions, in turn, permit the derivation of closed-form expressions for the wall transfer coefficients Nu_h and Nu_m (Sections 4.5, 4.6) as well as the vapor supersaturations near the OS-surface (Section 4.7).

4.5 Wall Heat Transfer in the Absence of Convection

Direct integration of the 'first integral' (4.2-1) provides the dimensionless heat transfer coefficient, Nu_h, defined by Eq. 4.3-2. One finds:

$$Nu_h = \frac{\frac{1}{1+\varepsilon}\cdot\left[\theta_e^{1+\varepsilon}-1\right]}{\theta_e - 1} \qquad (4.5\text{-}1)$$

While this ratio is always *unity* in the constant k-case ($\varepsilon=0$), it is seen to be 1.1 when

$$\varepsilon \approx 0.67,\ \theta_e \equiv \frac{T_e}{T_w} = 1.32$$

Thus, Eq. 4.5-1 permits straightforward calculation of the Fourier (gas) heat flux to the wall $-\ddot{q}_w$, at any ampoule temperature ratio, subject, of course, to the underlying assumptions discussed in Section 4.1.

4.6 Vapor Mass Transfer to the Wall in Absence of Convection

Direct integration of the 'first integrals' (4.2-1, 4.2-2), or differentiation of Eqs. 4.4-1, 4.4-2 followed by evaluation at $\eta=0$ provides the following closed-form result for the dimensionless vapor *mass* transfer coefficient:

$$Nu_m = \frac{\frac{1}{1+\varepsilon}\cdot\left[\theta_e^{1+\varepsilon}-1\right]}{\frac{1}{\beta}\left[\theta_e^{\beta}-1\right]}\cdot\left\{\frac{\theta_e^{\alpha_T}-\exp\left[-\mathcal{L}\left(1-\frac{1}{\theta_e}\right)\right]}{1-\exp\left[-\mathcal{L}\left(1-\frac{1}{\theta_e}\right)\right]}\right\} \qquad (4.6\text{-}1)$$

While, in the absence of the Soret effect (α_T=0) values of Nu_m are never very much greater than unity (see Fig. 4.5-1) it is seen that Nu_m can be as large as about 3 for $\theta_e \approx 1.32$ and α_T=10 when $\mathcal{L}$=60. (For comparison with the previous numerical results we note that Nu_m=1.41 for α_T=2.33.) Actually, Eq. 4.6-1 and Fig. 4.5-2 clearly reveal that, except very close to θ_e=1, the $\mathcal{L}$-dependence of Nu_m is negligible for $\mathcal{L}$-values of interest in these PVTOS applications.

Of theoretical interest (Rosner, 1980) is the enhancement in vapor mass transfer associated with the Soret effect, *i.e.*:

$$F(\text{Soret}) \equiv \frac{Nu_m}{(Nu_m)_{\alpha_T=0}} = \frac{\frac{1}{\beta_0}\cdot\left[\theta_e^{\beta_0}-1\right]}{\frac{1}{\beta}\left[\theta_e^{\beta}-1\right]}\cdot\frac{\theta_e^{\alpha_T}-\exp\left[-\mathcal{L}\left(1-\frac{1}{\theta_e}\right)\right]}{1-\exp\left[-\mathcal{L}\left(1-\frac{1}{\theta_e}\right)\right]} \qquad (4.6\text{-}2)$$

where β_0 is the value of the composite exponent β when α_T=0 (in the present case $\beta_0 \approx 1.17$). For values of θ_e 'large' enough to make $\exp\{-\mathcal{L}[1-(1/\theta_e)]\}$ negligible compared to unity (recall that $\mathcal{L} \approx 62$) we see that F(Soret) can be simplified to the interesting result:

$$F(\text{Soret}) \approx \left(1+\frac{\alpha_T}{\beta_0}\right)\cdot\theta_e^{\alpha_T}\cdot\frac{\theta_e^{\beta_0}-1}{\theta_e^{\beta_0+\alpha_T}-1} \qquad (4.6\text{-}3)$$

Note that if we insert β_0=1.17, β=3.17, $\alpha_T \approx 2$ and θ_e=1.32‡ we find F(Soret)≈1.28 in agreement with Fig. 4.6-2 and only slightly less than our earlier rough estimate (Section 2.1) F(Soret)≈1.32. Thus, under nominal PVTOS microgravity conditions, in the limit of no convection, the Soret effect would accelerate CuPc(v) transport to the OS-interface by about 30 percent over and above the contribution of Fick diffusion through the prevailing background gas mixture.

4.7 Supersaturations in Vapor Phase; s_{max} and $(\partial s/\partial\eta)_{\eta=0}$

As discussed in Section 2.5, we expect CuPc vapor *supersaturations* to hold the 'key' to OS-film quality, especially supersaturation behavior in the immediate vicinity of the OS-film itself. Using Eqs. 4.2-5, 4.4-2, and 2.4-4, we can derive a general expression for $s\{\theta; \theta_e; \mathcal{L}; \alpha_T; \beta_0\}$ from which we find:

---

‡ In this case, since $\mathcal{L} \approx 62$ we find

$$\exp\left[-\mathcal{L}\left(1-\frac{1}{\theta_e}\right)\right] \approx 3\times10^{-7}$$

which is certainly negligible compared to unity. Indeed, even if $\theta_e \to \infty$, F(Soret) would be limited to $[1+(\alpha_T/\beta_0)]$ or 2.71.

$$\left(\frac{ds}{d\eta}\right)_{\eta=0} = \frac{1}{1+\varepsilon}\left(\theta_e^{1+\varepsilon}-1\right)\left\{\frac{\theta_e^{\alpha_T} - \exp\left[-\mathcal{L}\left(1-\frac{1}{\theta_e}\right)\right]}{\frac{1}{\beta}\left[\theta_e^{\beta}-1\right]\cdot\exp\left[-\mathcal{L}\left(1-\frac{1}{\theta_e}\right)\right]} - (\alpha_T + L)\right\} \qquad (4.7\text{-}1)$$

which, for

$$\exp\left[-\mathcal{L}\left(1-\frac{1}{\theta_e}\right)\right] << 1 \text{ and } \alpha_T << L$$

simplifies to:

$$\left(\frac{ds}{d\eta}\right)_w \approx \frac{1}{1+\varepsilon}\left(\theta_e^{1+\varepsilon}-1\right)\left\{\frac{\theta_e^{\alpha_T}}{\frac{1}{\beta}\left[\theta_e^{\beta}-1\right]}\cdot\exp\left[\mathcal{L}\left(1-\frac{1}{\theta_e}\right)\right] - L\right\} \qquad (4.7\text{-}2)$$

revealing the very strong effect of θ_e and $\mathcal{L}$, and the lesser effects of α_T. This is shown graphically in Figs. 4.7-1a, b. For the particular case $\mathcal{L}$=60 with β_0=1.17, note that, for $\theta_e \approx 1.32$ values of $(ds/d\eta)_w$ exceed 2 million, so the vapor supersaturation grows quite rapidly with distance from the OS-film surface. Indeed, it is straightforward to calculate numerically the maximum values of the local supersaturation achieved within the ampoule, *i.e.*, s_{max}. These are shown plotted in Fig. 4.7-2a, b and reveal s_{max}-values near 6×10^4 for $\theta_e \approx 1.32$, $\mathcal{L} \approx 60$, β_0=1.17, $\alpha_T \approx 2$. Comparing $(ds/d\eta)_w$ with s_{max}, it is clear that the peak supersaturation is achieved quite close to the OS-film surface — *i.e.*, at small values of the dimensionless distance η. Clearly these supersaturation-values grow rapidly with increased θ_e-values (*e.g.* lower T_w-values).

4.8 Vapor Contribution to Mass Transfer in the VCE-Limit

It is interesting to ask what the vapor transport rates would be in the hypothetical case that the ampoule side-wall‡‡ were able to *prevent* any supersaturation in the vapor phase. In that case we have s=1 or *vapor condensate equilibrium* throughout the ampoule, and it is easy to show that this would *reduce* Nu_m-values by many orders of magnitude. This effect, too, is quite sensitive to L and rather less sensitive to α_T, as shown in Figs. 4.8-1a, b. Note that in such a case:

$$Nu_{m,eq} = \frac{1}{1+\varepsilon}\left(\theta_e^{1+\varepsilon}-1\right)(\alpha_T + L)\cdot\frac{\exp\left[-\mathcal{L}\left(1-\frac{1}{\theta_e}\right)\right]}{1-\exp\left[-\mathcal{L}\left(1-\frac{1}{\theta_e}\right)\right]} \qquad (4.8\text{-}1)$$

and, for, $\mathcal{L} \approx 62$, $\theta_e \approx 1.32$, $\varepsilon \approx 2/3$ we find that Nu_m is reduced from $Nu_{m,sf}$ (Eq. 4.6-1) by about the factor 5×10^{-6}. This is one indication that the potential effects of ampoule side-wall vapor

‡‡ or if homogeneous nucleation was rapid enough to form an equilibrium 'smoke' of CuPc(s) microparticles within the ampoule (see, *e.g.* Castillo and Rosner, 1989).

scavenging and/or homogeneous nucleation of CuPc(s)-'smokes' within the ampoule will be enormous, especially at low values of T_w and high source temperatures, T_e.

Indeed, the large difference between $Nu_{m,sf}$ and $Nu_{m,eq}$ betrays the upper limit to side-wall vapor scavenging; clearly most of the source vapor can be so scavenged, with only a small fraction showing up as OS-film growth at ⓦ .

4.9 Discussion, Implications

While convective flows due to buoyancy (*e.g.*, gravity, Section 3) and/or side-wall 'creep' (Section 2.4.3), as well as side-wall heat/mass transfer, will, of course, alter the idealized one-dimensional 'diffusional' results presented in this section, these results play a valuable role in demonstrating the relative importance of:

E1. Soret transport of CuPc(v)

E2. Variable thermophysical properties (k, D_v,ρ)

E3. Dimensionless heat of sublimation $\mathcal{L} \equiv \Lambda/(RT_w)$

E4. Ampoule source: sink temperature ratio

and providing asymptotically 'exact' results that can be used to check more complex computational fluid dynamics codes (Section 3) in the limits of vanishing buoyancy ($Ra_h \rightarrow 0$), vanishing side-wall 'creep', and vanishing side-wall heat/mass transfer.

5. CONCLUSIONS, IMPLICATIONS, RECOMMENDATIONS

5.1 Summary of Present Program

During this pilot program (7 April – 31 August 1988; with no-cost extension to January 6, 1989) we have established that under typical PVTOS-ampoule conditions:

C1 Side-wall 'creep' associated with the wall temperature gradient will drive a gas flow within PVTOS ampoules irrespective of gravity. Even in ground-based experiments, this side-wall 'slip' effect, evidently not previously considered by the PVT-CVT community, is not negligible compared to bouyancy-driven convection (Section 2.4.3).

C2 While the creeping gas flow within the ampoule is near-continuum, the temperature gradients are such that the usual Stokes-Fourier constitutive laws for the stresses and heat flux may need to be supplemented – *i.e.*, ordinary Navier-Stokes-Fourier 'closure' is probably inadequate (Section 2.4.3).

C3 Owing to the large molecular mass disparity between the organic vapor (*e.g.*, CuPc(g) and the background gas, Soret (thermal-) diffusion is expected to be appreciable (*ca.* 30% augmentation in OS-growth rate in the absence of convection (*i.e.*, over that of Fick diffusion alone; Section 2.1).

C4 Again, owing to large molecular weight disparities between the organic vapor (*e.g.*, 'CuPc'(g)) and within the background gas mixture itself (*e.g.*, H_2, Xe) the diffusivity ratios Pr (momentum/heat) and Sc (momentum/mass) depart appreciably from unity. Indeed, the thermal diffusivity of such mixtures is expected to be about one decade greater than the Fick diffusivity for the organic vapor (Section 2.3), with a significant influence on the vapor-phase supersaturations (Sections 2.5, 4.7).

C5 The effects of Stefan flow and departures from vapor/solid phase equilibrium at the source ⓔ and sink ⓦ gas/solid interfaces are probably negligible (Sections 2.4.1, 2.4.2). Soret separation of the background gas itself may have to be included in extreme cases (Section 2.2).

C6 Very large vapor-phase supersaturations (above 10^4) are anticipated within the ampoule. This probably implies the presence of non-negligible vapor-phase clustering (*i.e.* formation of 'CuPc'-n-mers (n=2, 3,...)), with an attendant influence on film quality (Sections 2.5, 4.7). Dimensionless supersaturation gradients in the immediate vicinity of the surface exceed 10^6, so that smooth, dense films may be unstable at sufficiently high T_e/T_w-values (Sections 2.5, 4.7).

C7 It is possible to make numerical predictions of the creeping axisymmetric steady gas flows expected under these extreme $\Delta T/T$-conditions, allowing for side-wall scavenging of heat and vapor mass (Section 3), and including realistic 'creep' boundary conditions (Section 2.4.3), departures from Stokes-Fourier 'closure', as well as gravitational forces.

C8 A rational formalism can now be implemented (Garcia-Ybarra and Rosner, 1989) to predict the Fick- and Soret- diffusivity of rapidly tumbling "platelet" macromolecules (of the CuPc(g)-type) in a low molecular weight background gas.

These findings put us in a unique position to make dramatic gains in the understanding/control of PVTOS processes – both under conditions of microgravity, and in ground-based (± 1g (Earth)) experiments (See Section 5.2 below).

5.2 Recommended Extensions

5.2.1 T1: Side-wall thermal creep in PVTOS ampoules

As pointed out in Section 2.4.3, in this pilot program we have discovered that under present PVTOS-ampoule conditions (low pressure, high side-wall temperature gradients intermediate ampoule aspect ratio) the phenomenon of side-wall thermal 'creep' (of the gas) will be an important 'cause' of convection, *irrespective of gravity*. This does not seem to have been previously appreciated and, obviously warrants careful study in our follow-on program. We will also investigate the extent to which Soret-induced *composition* gradients in the effective background gas will contribute to the expected side-wall 'creep'.

5.2.2 *T2: Role of ampoule sidewall 'scavenging' of CuPc-vapor and energy*

Our preliminary numerical computations and ancillary theoretical studies suggest that 'parasitic' removal of CuPc(g) and energy by the ampoule sidewalls, especially in the vicinity of the growing organic film, can have an enormous influence on local supersaturations and, hence, presumably, crystal morphology, quality, and spatial nonuniformity. It is interesting that modest sidewall *energy* loss opens the possibility of ground-based natural convection even at Rayleigh[‡‡] numbers of order 1–10, whereas ground-based experiments in a hypothetical ampoule with perfectly 'adiabatic' walls would be expected to be free of convective effects at such low Rayleigh numbers. A better definition of actual mass and heat transfer conditions at the ampoule sidewalls will clearly be necessary in future research — indeed, it is possible that some deliberate modification in the sidewall thermal condition for a given aspect ratio would suppress natural convection and approximate 'microgravity' conditions even in ground-based crystal growth experiments.

5.2.3 *T3: Kinetic theory of rapidly tumbling nonspherical macromolecules*

In contrast to the limiting case explicitly dealt with in Garcia-Ybarra and Rosner (1988), *viz.*, a macromolecule which is unable to respond rotationally on the time scale of successive carrier gas impacts, plate-like macromolecules such as "CuPc" under PVTOS conditions would rotate many times on the time scale of successive molecular impacts, thereby altering the effective cross-section of the macromolecule. By exploiting the fact that both of these time scales are short compared to the 'relaxation' time associated with a change in the macromolecule rotational or translational motion, it is possible to develop a rational theory of the relevant effective cross-section, as well as the important associated transport properties D ("Brownian" [translational]) diffusivity, and α_T (thermal [Soret]) diffusion factor (Rosner, 1980). Useful corollaries would be expressions for the binary collision rates between CuPc-molecules (and clusters thereof) in the vapor phase, and between the vapor phase CuPc molecules and the crystal surface.

5.2.4 *T4: Effects of vapor phase clustering on PVTOS-crystal quality*

Our quantitative estimates of local supersaturations and residence times in PVTOS-ampoules opens the door to an evaluation of the probability and consequences of vapor phase clusters (*e.g.*, 'sheet-like' or 'stack-like') of CuPc molecules in the immediate vicinity of the growing organic solid film. For this purpose, we make use of our new cross-section estimates

---

‡‡ This group is readily shown to dictate the behavior of variable density Newtonian fluids in a gravity field (see, *e.g.*, Rosner, 1986)

(T2) as well as thermochemical estimates of the stability of (CuPc) n-mers, hopefully available *via* independent chemical studies in the recent literature, suitably extrapolated.

5.2.5 *T5: Morphological stability of organic films grown in PVT-ampoules*

Using both continuum simulations and Monte-Carlo (discrete) simulations it would be instructive to study the conditions under which films grown in the simultaneous presence of Soret diffusion, Fick diffusion and natural convection are morphologically stable with respect to local growth disturbances. Such studies would be natural extensions of work that we have already initiated (under AFOSR and DOE support) on the morphological stability of powdery deposits (see, *e.g.*, Garcia-Ybarra *et al.*, 1988; and Tassopoulos *et al.*, 1988) in the presence of thermophoresis

5.2.6 *T6: Develop/Exercise Capability to Make Axisymmetric Natural Convection Ampoule Calculations for realistic Geometries, Boundary Conditions and Thermophysical Properties*

While we have been able to investigate the simplest geometries and thermal boundary conditions in the presence[†††] of an appreciable Soret effect, for realistic non-unity Prandtl and Schmidt numbers and *without* making the Boussinesq approximation, it is clear that with further development of our axisymmetric Navier-Stokes code it will be possible to carry out simulations of increasing realism (*i.e.* fewer 'idealizations'), including transients, if necessary. Indeed, as pointed out in Section 2.4.3, we will also be able to generate (apparently for the first time) solutions which transcend ordinary Navier-Stokes gas dynamics in the sense that we will include the necessary Burnett terms in the stress law and generalized heat flux. This capability could be extremely valuable in guiding and interpreting future PVTOS experiments — both ground-based and microgravity.

5.3. Summary of Phase II Program (commencing *ca.* January 1, 1989)

In summary, as partially anticipated in our earlier documents, our Phase I (Pilot) studies have set the stage for more comprehensive Phase II theoretical studies, including:

II.1 Evaluate the gas kinetic phenomena of non-isothermal side-wall gas 'creep' and 'thermal stress convection' under realistic PVTOS ampoule conditions, both in the presence and absence of gravity.

II.2 Evaluate the role of ampoule "sidewall-scavenging" of *heat* and CuPc-*mass* on crystal growth conditions near the organic film interface. Explore the possibility of altering sidewall conditions to simulate the effects of microgravity in ground-based experiments.

[†††] Ironically, these important effects are all neglected in the previous work of T.L. Miller (1986).

II.3 Extend our earlier research on the kinetic theory of nonspherical macromolecules (Garcia-Ybarra and Rosner, 1988) to cover the case of rapidly tumbling sheet-like molecules (*e.g.*, CuPc). Infer Fick and Soret diffusivities as well as collision rates.

II.4 Quantitatively investigate likelihood, extent and consequences of vapor phase clustering of CuPc-molecules in the supersaturated vapor above the growing organic film.

II.5 Assess the clustering consequences of local CuPc-vapor supersaturations on the stability of the growing film interface (quasi-continuum model) as well as Monte-Carlo (molecular-level model) simulations of the condensation, surface diffusion, and crystallization of large platelet molecules arriving from the vapor phase.

II.6 Initiate a sequence of more realistic numerical calculations of axisymmetric natural convection in nonisothermal ampoules — including transient effects, non-Fickian diffusion, experimentally measured surface temperatures, and high resolution in the vicinity of the growing film.

In the course of this follow-on program, we would locate and mobilize and/or rationally estimate property-data needed to fully exploit the abovementioned microscopic mathematical modeling capabilities. Based on results of microgravity experiments (including STS-26, October 1988), ground-based (lab) experiments, and the insights from our theoretical studies, we may be able to recommend optimal experimental conditions for growth of highly oriented organic films under microgravity conditions and, perhaps, also under cleverly controlled, ground-based experimental conditions.

Acknowledgements:

This program was supported at Yale under NASA grant No. NAG 3-898, and through non-personal service contracts with Drs. D.E. Rosner and D.E. Keyes, PR 311494, Order No. C-21892-K. The program monitor at NASA-Lewis Research Center was Dr. Gary D. Roberts (Materials Engineer, Metals Science Branch, Bldg 105, Rm 204) and our technical contact with 3M was Dr. Mark K. Debe, Science Research Lab., 3M Center.

It is a pleasure to acknowledge the contributions to this pilot program made by Drs. P. Garcia-Ybarra (kinetic theory of tumbling platelet molecules; Sections 2.1, 2.3), J. Castillo (parametric studies governing the one-dimensional diffusion limit; Section 4), and K.S. Kim (numerical studies of natural convection in finite cylindrical ampoules; Section 3). Thanks are also due to M. Smooke, G.A. Bird, J. Fernandez de la Mora for helpful discussions, and to J. Collins and P. Bauwens for their assistance in the editing and production of this final report.

6. REFERENCES

Bonderman D., Cater E.D., and Bennet W.E. (1970), "Vapor Pressures, Mass, Spectra, Magnetic Susceptibilities and Thermodynamics of Some Phthalocyanine Compounds" *J. Chem. Engrg. Data* (ACS) **15**, 396-400

Brown C.J. (1968), "Crystal Structure of β-Copper Phthalocyanine", *J. Chem Soc.* (A) 2488-2493

Castillo J.L., and Rosner D.E. (1989), "Theory of Surface Deposition from a Unary Dilute Vapor-Containing Stream Allowing for Condensation within the Laminar Boundary Layer", *Chem. Engrg Sci.* (in press)

Catton I. (1972), "Effect of Wall Conduction on the Stability of a Fluid in a Rectangular Region Heated from Below", *J. Heat Mass Transfer* **94**, 446-452

Charlson G.S., and Sani R.L. (1971), "On Thermoconvective Instability in a Bounded Cylindrical Fluid Layer", *Int. J. Mass Transfer* **14**, 2157-2160

Curtis A.R., Powell M.J., and. Reid J.K.(1974), "On the Estimation of Sparse Jacobian Matrices", *J. Inst. Math. Appl.* **13**, 117-119

Debe M.K. (1984), "Extracting Physical Structure Information from Thin Organic Films with Reflection Absorption Infrared Spectrometry", *J. Appl. Phys.* **55** (9), 3354-3366

Debe M.K. *et al.* (July/August, 1987), "Vacuum Outgassing and Gas Phase Thermal Conduction of a Microgravity Physical Vapor Transport Experiment", *J. Vac Tech.* A5(4) 2406-2411

Friedlander S.K. (1977) **Smoke, Dust and Haze — Fundamentals of Aerosol Behavior**, New York: J. Wiley

Garcia-Ybarra P., and Rosner, D.E. (1988), "Thermophoretic Properties of Small Nonspherical Particles and Large Nonspherical Molecules", *AIChE J.* (in press)

Garcia-Ybarra P., and Rosner, D.E. (1989), "Transport Properties of Rapidly Tumbling Nonspherical Macromolecules", (in preparation)

Gosman A.D.,Pun W.M., Runchal A.K., Spalding D.B., and Wolfshtein M. (1969), **Heat and Mass Transfer in Recirculating Flows**, Academic Press, New York

Kee R.J., Miller J.A., and Jefferson T.H. (March, 1980), "CHEMKIN: A General-Purpose, Transportable, Fortran Chemical Kinetics Code Package", *Technical Report SAND80-8003*, Sandia National Laboratories

Kee R.J., Warnatz J., and Miller J.A. (March, 1983), "A FORTRAN Computer Code Package for the Evaluation of Gas-Phase Viscosities, Conductivities, and Diffusion Coefficients", *Technical Report SAND83-8209*, Sandia National Laboratories

Kennard E.H. (1938), **Kinetic Theory of Gases**, McGraw-Hill, N.Y.

Keyes D.E, and Smooke M.D. (1987), "Flame Sheet Starting Estimates for Counterflow Diffusion Flame Problems", *J. Comp.Phys.* **72**, 267-288.

Kogan M.N. (1973), "Molecular Gas Dynamics", in Vol. 5, *Annual Reviews of Fluid Mechanics*, Annual Reviews Inc., Palo Alto, CA , 383-404

Kogan M.N. (1986), "Non-Navier-Stokes Gas Dynamics and Thermal Stress Phenomena", in **Proc. 15th Int. Symp. Rarefied Gas Dynamics**, Vol.**1**, B.G. Tuebner, Stuttgart, 15-24

Kramers H.A., and Kistemaker J. (1943), "On the Slip of a Diffusing Gas Mixture along a Wall", *Physica* (Martinus Nijhoff, The Hague) **10**, No.8, 699-713

Miller T.L. (1986), "Numerical Modeling of PVT in a Vertical Cylindrical Ampoule, with and without Gravity", NASA TP 2620

Müller G., and Neuman G. (1983), "Investigation of Convective Flows in Model Systems of Directional Solidification Configurations", in *Proc. of the Fourth Eur. Symp. Mater. Sci. Under Microgravity*, ESA (Europ. Space Agency) SP-191, Paris 285-294

Ostrach S. (1982), "Low Gravity Fluid Flows", *Ann. Rev.Fluid Mechanics* (Annual Reviews, Palo Alto, CA) **14**, 313-345

Puri I.K., Seshadri K., Smooke M.D., and Keyes D.E. (1987), "A Comparison between Numerical Calculations and Experimental Measurements of the Structure of a Counterflow Methane-Air Diffusion Flame", *Comb. Sci. Tech.* **56**, 1-22

Rosenberger F. (1979) **Fundamentals of Crystal Growth I: Macroscopic Equilibrium and Transport Concepts**, Springer-Verlag, Berlin-Heidelberg-New York

Rosner D.E. (1966), "Effects of the Stefan-Nusselt Flow on the Apparent Kinetics of Heterogeneous Chemical Reactions in Forced Convection Systems", *Int. J. Heat & Mass Transfer* **9**, 1233-1253

Rosner D.E. (1980), "Thermal (Soret) Diffusion Effects on Interfacial Mass Transport Rates", *J. PhysicoChemical Hydrodynamics* **1**, 159-185

Rosner D.E. (1985), "Mass Transfer across Combustion Gas Thermal Boundary Layers — Power Production and Materials Processing Implications", in **Heat Transfer in Fire and Combustion Systems**, HTD **45** (Law C.K., Jaluria Y., Yuen W.W. and Miyasaka K., eds.) ASME, NY, N.Y. 3-8

Rosner D.E. (1986) **Transport Processes in Chemically Reacting Flow Systems**, Butterworths (Stoneham, MA); 2nd printing 1988

Rosner D.E. (1988), "Experimental and Theoretical Research on the Deposition Dynamics of Inorganic Compounds from Combustion Gases", Invited paper for the B. G. Levich Memorial Volume of *PhysicoChemical Hydrodynamics* (Vol. **10**, No.5; in press)

Rosner D.E., Chen B.K., Fryburg G.C., and Kohl F.J. (1979), "Chemically Frozen Multicomponent Boundary Layer Theory of Salt and/or Ash Deposition Rates from Combustion Gases", *Comb. Sci. & Tech.* **20**, 87-106

Rosner D.E., and Epstein M. (1968), "Fog Formation Conditions near Cool Surface", *J. Colloid & Interface Sci.* **28**, 60-65

Smooke M.D., Turnbull A.A., Mitchell R.E., and Keyes D.E. (1987), "Solution of Two-Dimensional Axisymmetric Laminar Diffusion Flames by Adaptive Boundary Value Methods", in **NATO Advanced Research Workshop on Mathematical Modeling in Combustion**, Brauner C.M. and Schmidt-Lainé C. ed., NATO.

Svehla R. (1962), NASA TR R-132Svehla R.A. (1962), NASA TR R-132 (N63-22862), "Estimated Viscosities and Thermal Conductivites of Gases at high Temperatures

Tassopoulos M., O'Brien J.A., and Rosner D.E. (1988), "Theoretical Approach to Establish Particle Deposition Mechanism/Deposit Microstructure Relationships", 1988 Annual AIChE Mtg, Washington, D.C., Nov.27-Dec.2

7. NOMENCLATURE

Roman

B	dimensionless 'blowing' parameter (Rosner, 1986)
$\bar{c}_i$	mean thermal speed of molecules of species i
c_p	molar heat capacity
Dam	Damköhler number
D_v	Fick diffusion coefficient for vapor in prevailing gas mixture
g	acceleration due to gravity
Gr	Grashof number for heat transfer, $g\beta\Delta TL^3/\nu^2$
j_v''	vapor diffusion mass flux
k_B	Boltzmann constant
k_h	thermal conductivity
Kn	Knudsen number
L	axial length of cylindrical PVT-ampoule
$\mathcal{L}$	dimensionless heat of sublimation for organic solid $\Lambda/(RT_w)$
l	gas mean free path
Le	Lewis number; diffusivity ratio D_v/α_h
$\overline{M}$	mean molecular mass of the mixture
M_i	molecular weight of species i
n	$\equiv$ d ln D_v/d ln T ($n_c \equiv$ n-1)

Nu_h	Nusselt number (dimensionless *heat* transfer coefficient)
Nu_m	Nusselt number (dimensionless *mass* transfer coefficient)
p	total pressure
Pe	Peclet number
Pr	Prandtl number, $\nu_{mix}/\alpha_{h,mix}$
$\ddot{q}_F$	Fourier energy flux
R	universal gas constant
r	molecular mass difference parameter
r	radial coordinate
Ra	Rayleigh number
s	local vapor supersaturation
Sc	Schmidt number ν_{mix}/D_{v-mix}
T	local absolute temperature
t	time
y_i	mole fraction of chemical species i
z	axial coordinate measured from growing film surface

Greek

α_{evap}	evaporation coefficient
α_h	thermal diffusivity $(k/(\rho c_p))$
α_T	thermal diffusion (Soret) factor
β	thermal expansion coefficient of ideal gas mixture (1/T)
Δ	'change in' operator
ϵ	d ln k / d ln T
ϵ_{ij}	energy wall-depth parameter for the interaction of molecules of species i and j
η	dimensionless distance from organic film, z/L
Λ	heat of solid sublimation
μ	dynamic viscosity
ν	momentum diffusivity (kinematic viscosity) μ/ρ
θ	temperature ratio, T/T_w
ρ	mass density of mixture
σ_{ij}	molecule size parameter
ψ	axisymmetric flow stream function
Ω	local measure of fluid vorticity (rotation rate)
Ω'	radially normalized Ω

ω_v	local mass fraction of vapor in mixture

Subscripts

c	pertaining to cell (Section 3.8)
cr	critical
eq	pertaining to local vapor/solid equilibrium
evap	evaporation
g	pertaining to *gas* mixture
h	pertaining to heat transfer
het	pertaining to the heterogeneous (vapor/solid interface) processes
i	species i
ij	interaction between species i and j
m	pertaining to mass transfer
max	maximum value
mix	pertaining to the prevailing gas mixture
rot	pertaining to molecular rotation
v	vapor
w	evaluated at vapor/solid interface ("wall")
ω	pertaining to mass fraction of vapor
Ω	pertaining to local measure of fluid vorticity

Abbreviations

3M	3M Corporation (St. Paul, MN)
BC	boundary conditions
CuPc	copper phthalocyanine
CVD	chemical vapor deposition
CVT	chemical vapor transport
grad	spatial gradient
iso	operator on scalars defined, *e.g.*, in Gosman *et al.* (1969)
LVSE	local vapor/solid equilibrium
ODE	ordinary differential equation
OS	organic solid(s)
PVT	physical vapor transport
$\mathcal{AR}$	aspect ratio of ampoule (L/d_w)
sf	source (sink)-free
SNIF	slow non-isothermal flow

8. LIST OF FIGURES

9. LIST OF TABLES

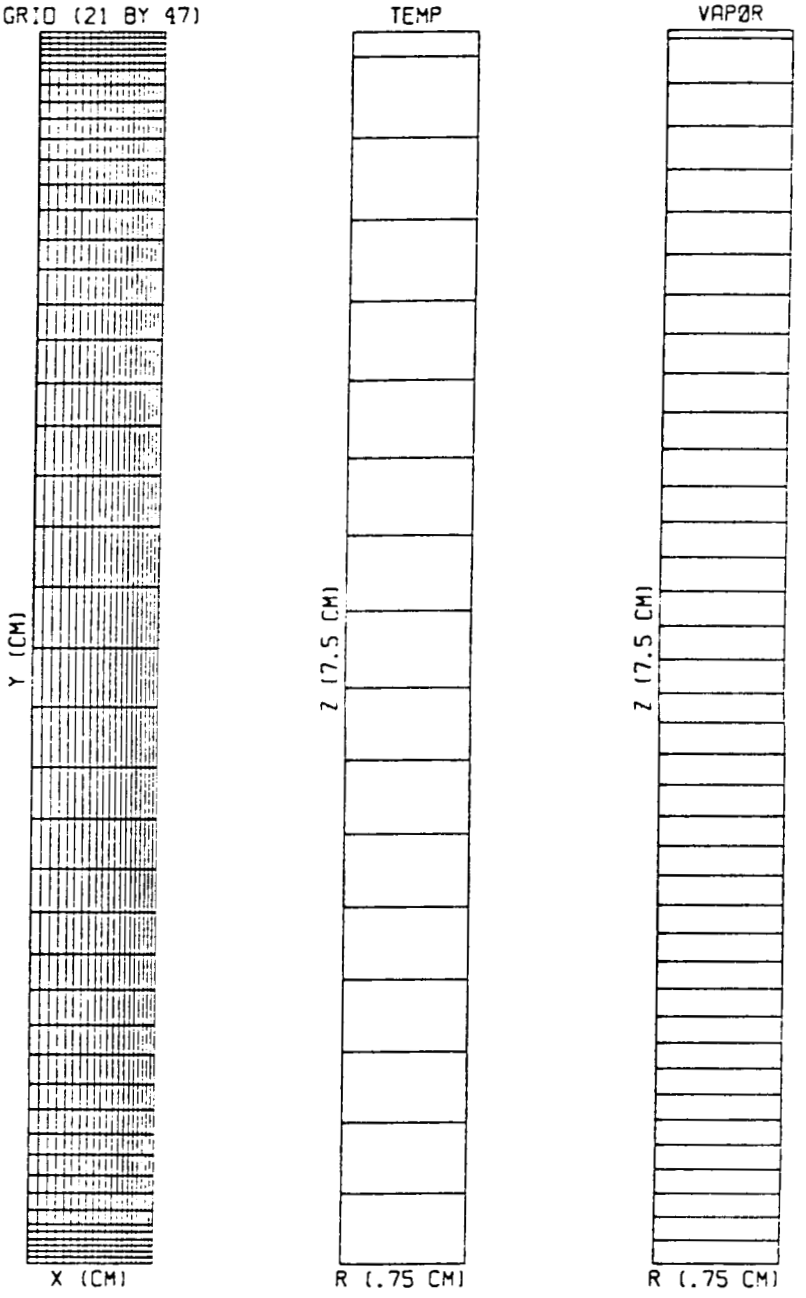

3.7-1

Grid, temperature contours T = 510 (10) 673 K and CuPc vapor contours ω_v = 1.24 x 10^{-9} (10^{-4}) 3.82 x 10^{-3} at standard operating conditions (3.2 Torr)

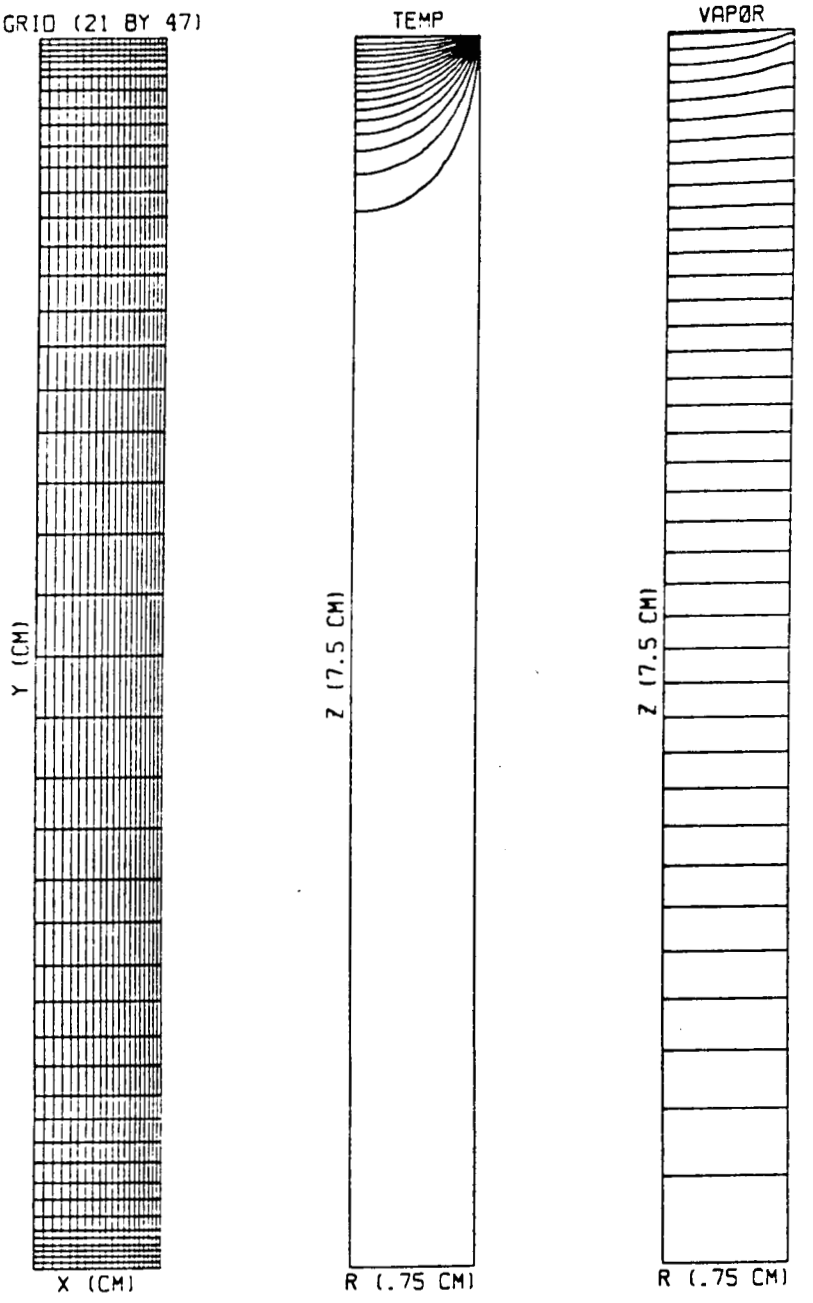

3.7-2

Grid, temperature contours T = 510 (10) 673 K and CuPc vapor contours ω_v= 1.24 x 10^{-9} (10^{-4}) 3.82 x 10^{-3} at standard operating conditions with parasitic heat loss

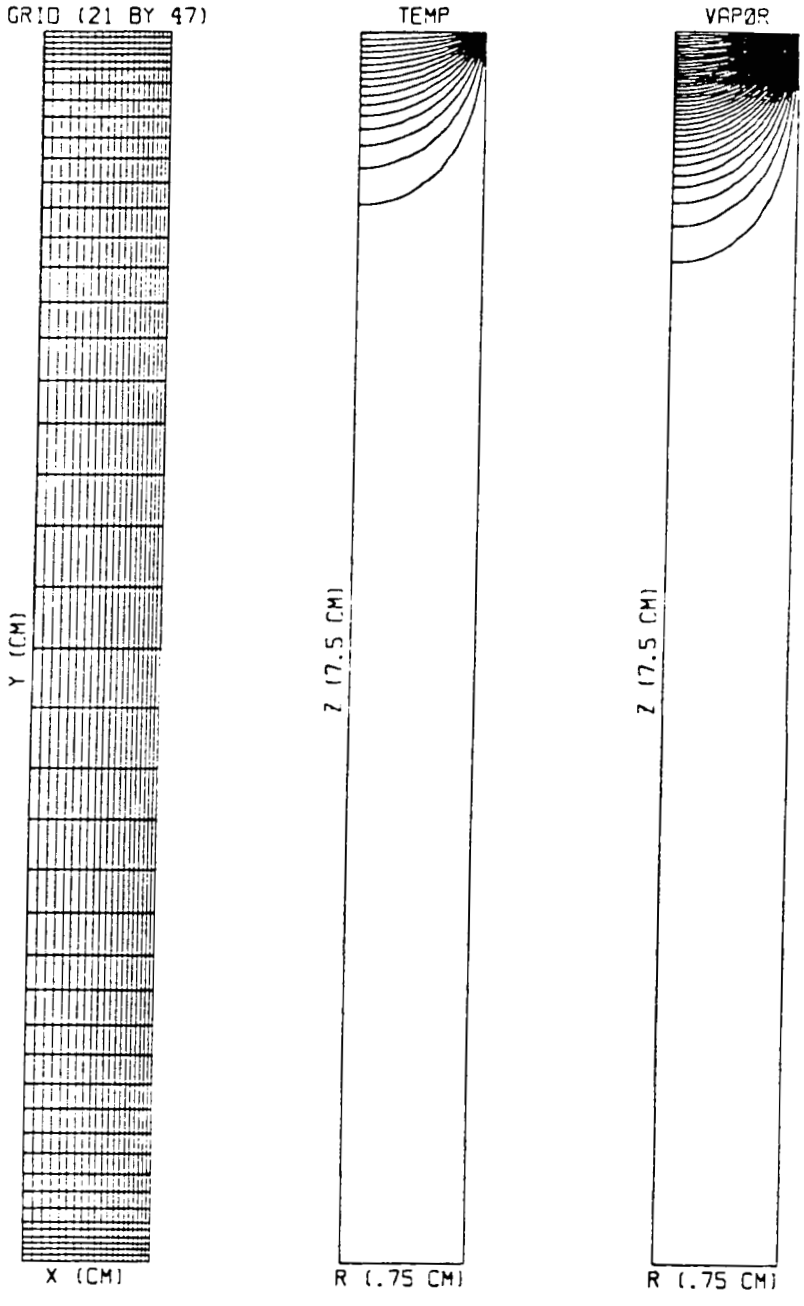

3.7-3

Grid, temperature contours T = 510 (10) 673 K and CuPc vapor contours $\omega_v = 1.24 \times 10^{-9}$ (10^{-4}) 3.82×10^{-3} at standard operating conditions with parasitic heat loss and equilibrium vapor boundary conditions on the side-walls

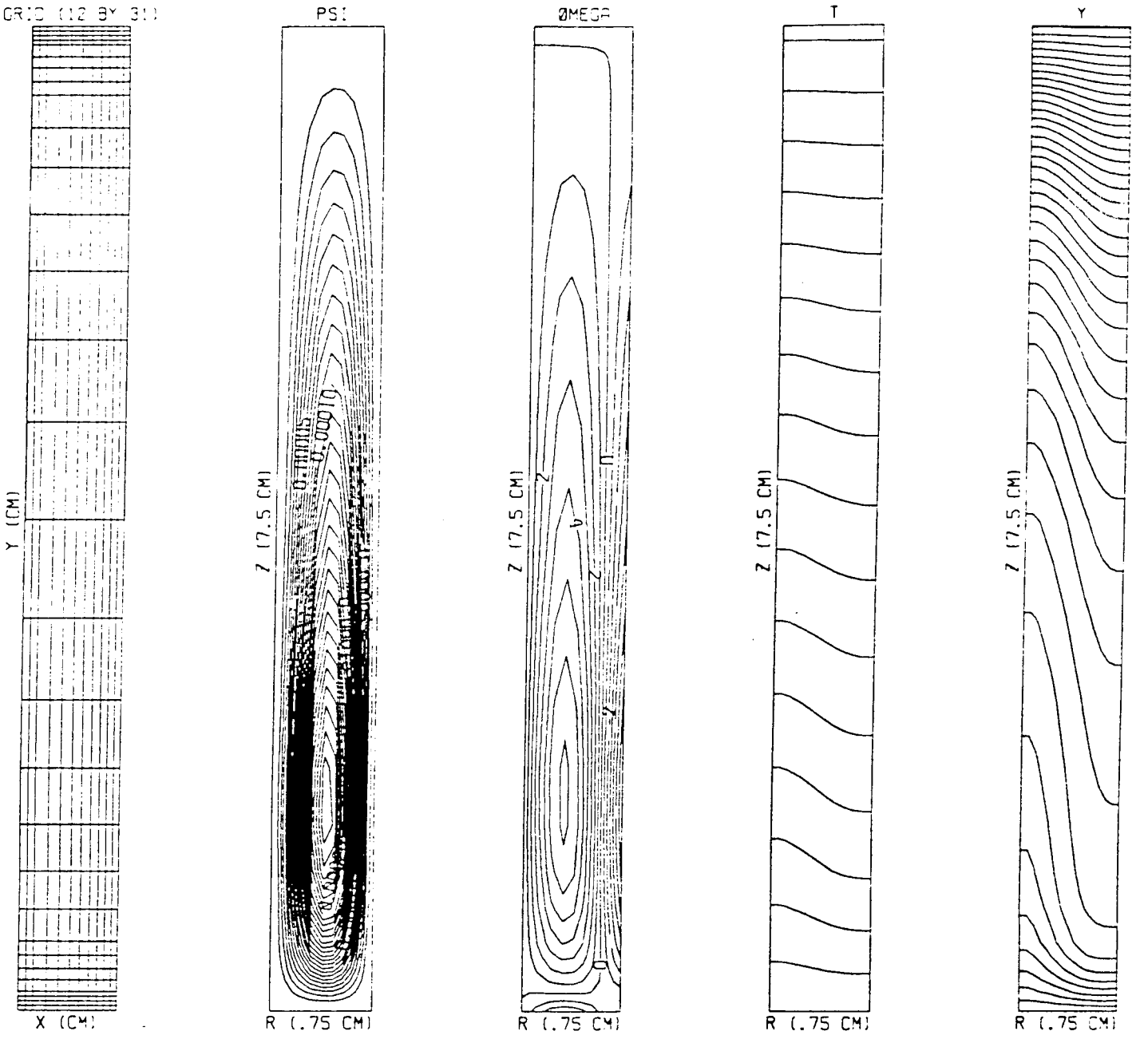

3.7-4 Grid, Stream function contours, vorticity contours, temperature contours T = 510 (10) 673 and CuPc vapor contours ω_v= 1.24x10^{-9} (10^{-4}) 3.82x10^{-3} at p_0 = 3.2 x 10^3 Torr (=4.2 atm)

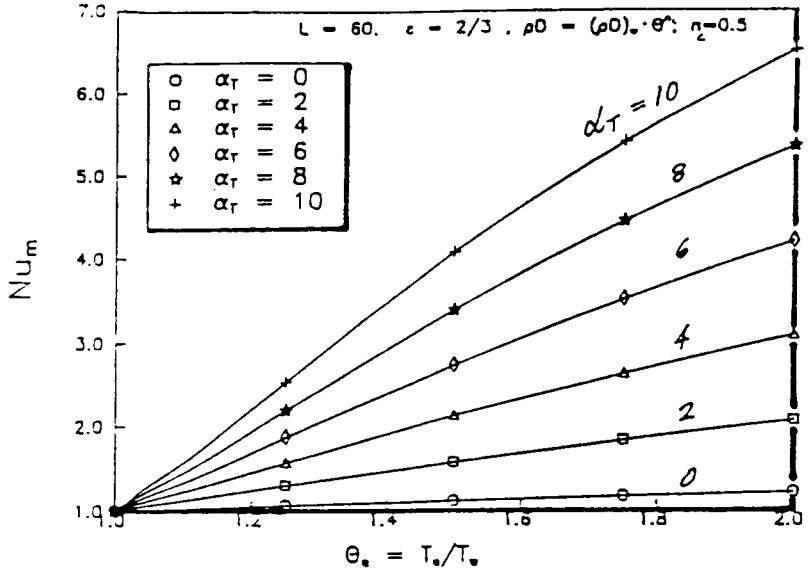

4.5-1 Dependence of dimensionless *mass* transfer coefficient, Nu_m, on wall temperature ratio for several values of the organic vapor Soret coefficient ($\mathcal{L}$=60, ε=2/3, n_c=1/2)

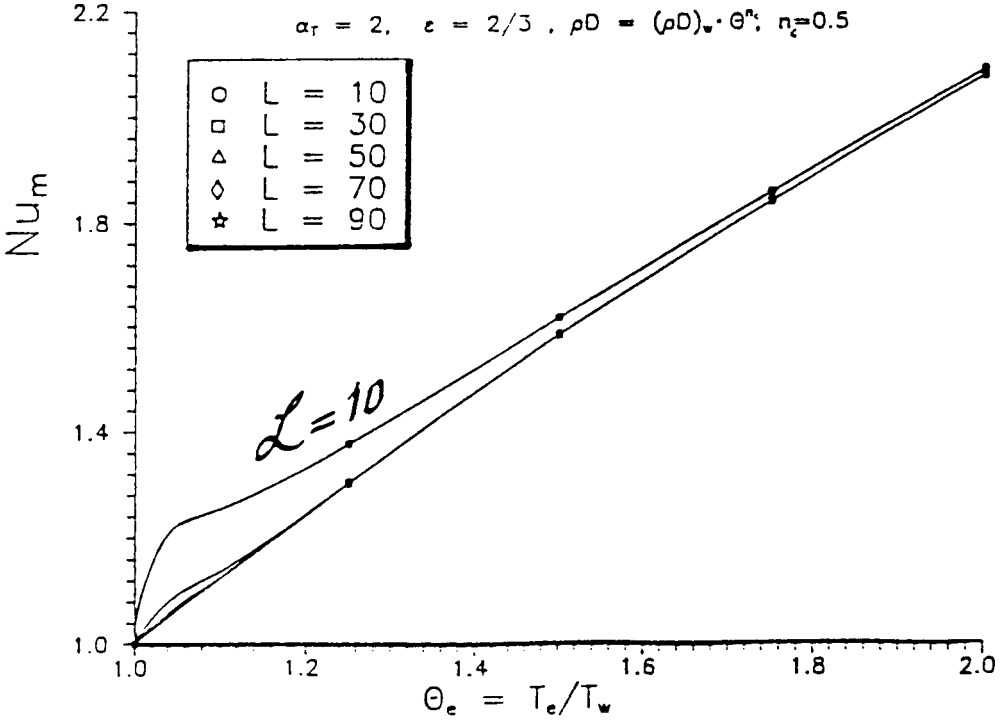

4.5-2 Dependence of dimensionless *mass* transfer coefficient, Nu_m, on wall temperature ratio T_e/T_w for several values of the dimensionless heat of sublimation $\mathcal{L}$ (α_T=2, ε=2/3, n_c=1/2)

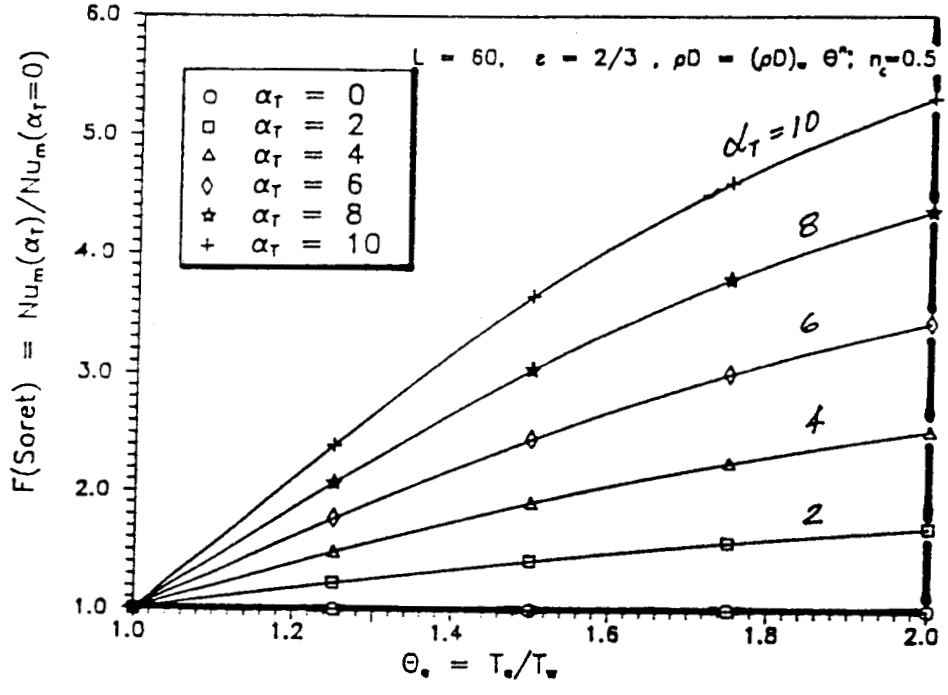

4.5-3 Soret-induced vapor mass transfer augmentation factor, F(Soret), vs. wall temperature ratio T_∞/T_w for several values of the Soret factor α_T ($\mathcal{L}$=60, ε=2/3, n_c=1/2)

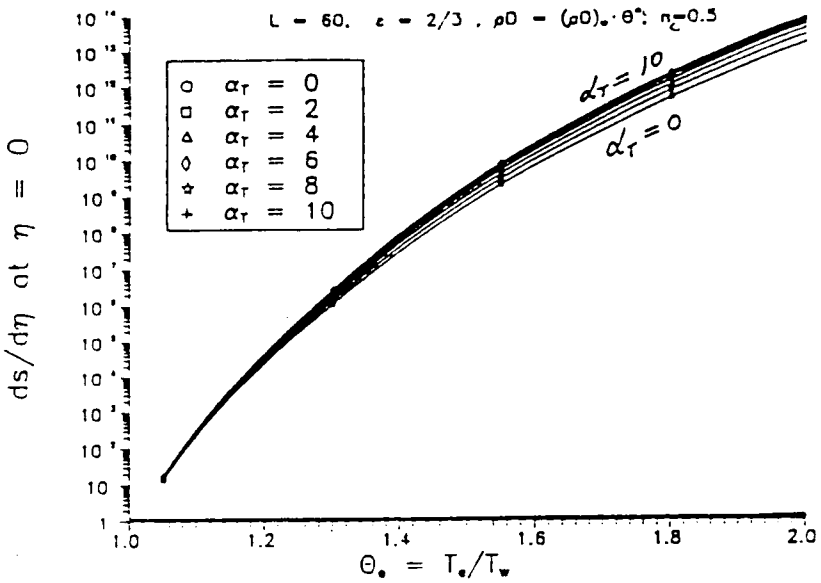

4.7-1a Dependence of vapor supersaturation gradient at wall, $(ds/d\eta)_w$, on wall temperature ratio T_e/T_w for several values of the Soret factor α_T ($\mathcal{L}$=60, ε=2/3, n_c=1/2)

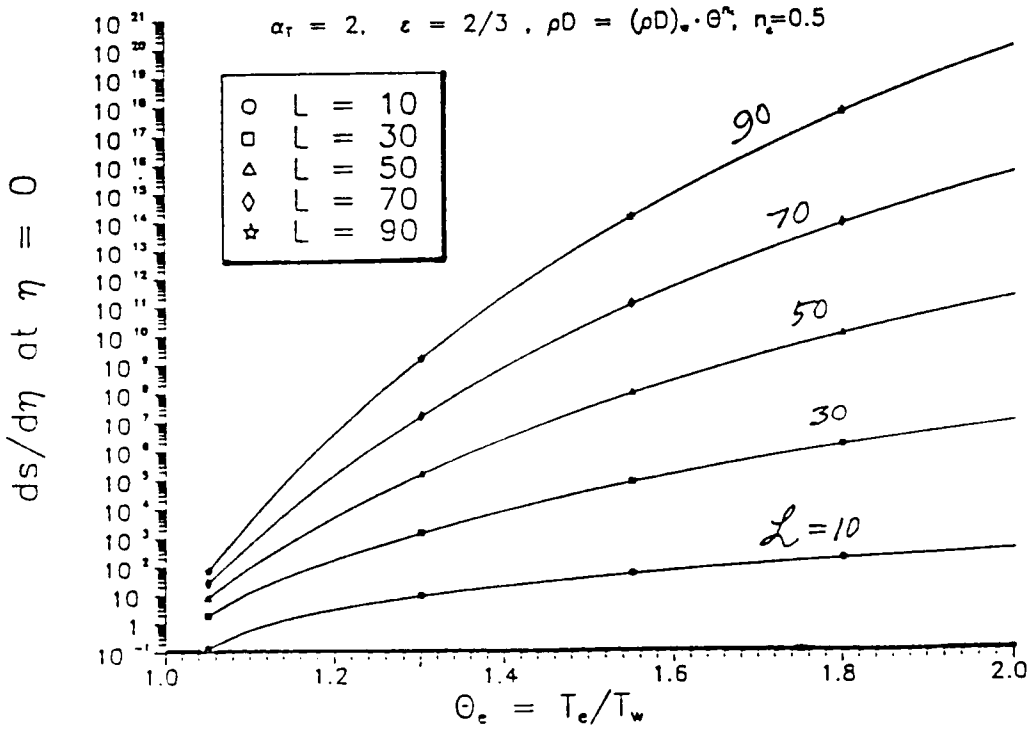

4.7-1b Dependence of vapor supersaturation gradient at wall, $(ds/d\eta)_w$, on wall temperature ratio T_e/T_w for several values of the dimensionless heat of sublimation $\mathcal{L}$ (α_T=2, ε=2/3, n_c=1/2)

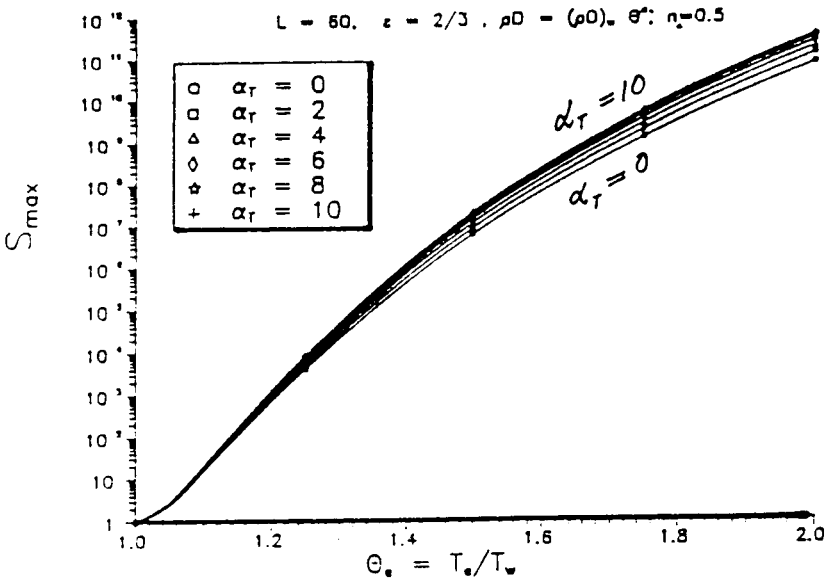

4.7-2a Dependence of maximum vapor phase supersaturation, s_{max}, on wall temperature ratio T_e/T_w for several values of the Soret factor α_T ($\mathcal{L}$=60, ε=2/3, n_c=1/2)

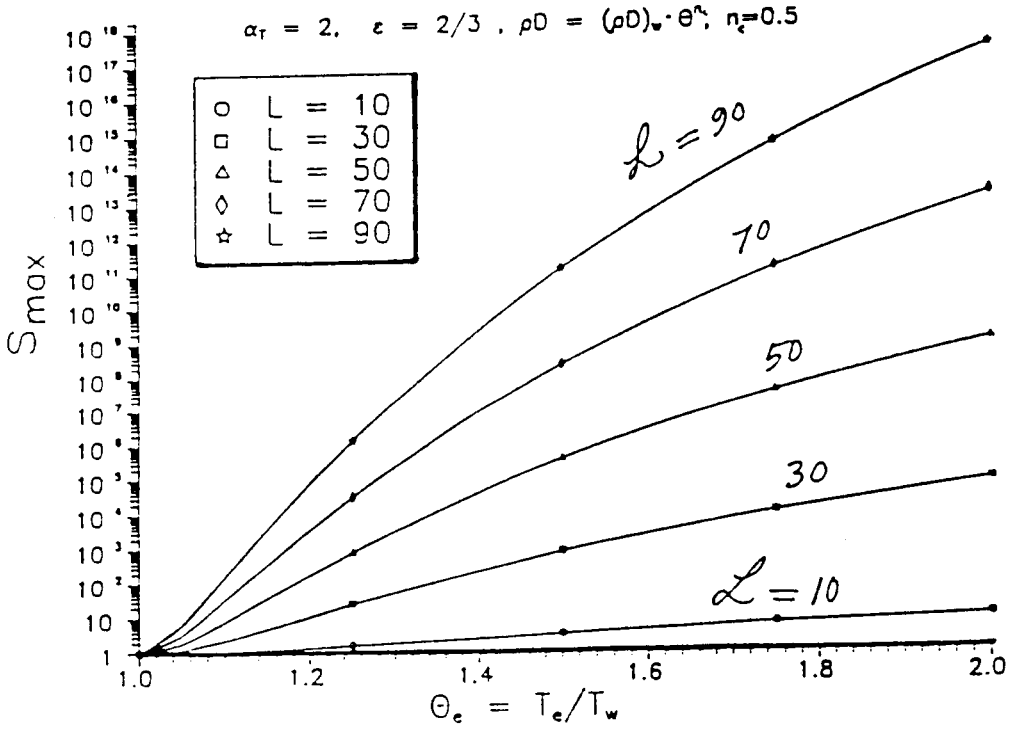

4.7-2b Dependence of maximum vapor phase supersaturation, s_{max}, on wall temperature ratio T_e/T_w for several values of the dimensionless heat of sublimation $\mathcal{L}$ (α_T=2, ε=2/3, n_c=1/2)

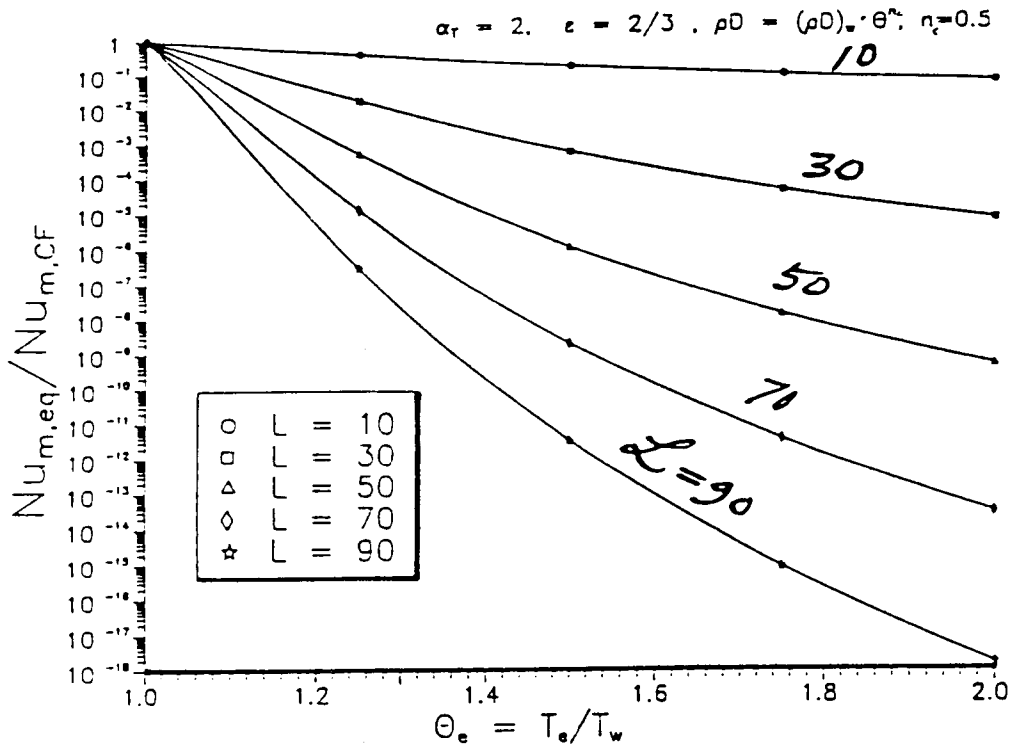

4.8-1a Ratio of the local equilibrium vapor flux to the 'sink free' vapor flux at ⓦ as a function of wall temperature ratio T_e/T_w for several values of the dimensionless heat of sublimation $\mathcal{L}$ (α_T=2, ε=2/3, n_c=1/2)

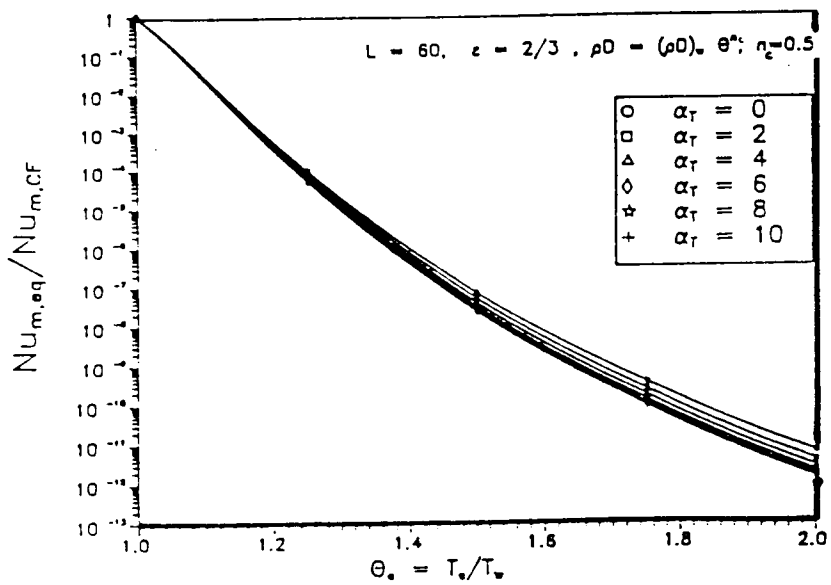

4.8-1b Ratio of the local equilibrium vapor flux to the 'sink free' vapor flux at ⓦ as a function of wall temperature ratio T_e/T_w for several values of the Soret factor α_T ($\mathcal{L}$=60, ε=2/3, n_c=1/2)

NASA
National Aeronautics and Space Administration

Report Documentation Page

1. Report No.	2. Government Accession No.	3. Recipient's Catalog No.
NASA CR-185122		

4. Title and Subtitle	5. Report Date
Theoretical Studies in Support of the 3M-Vapor Transport (PVTOS-) Experiments	July 1989
	6. Performing Organization Code

7. Author(s)	8. Performing Organization Report No.
Daniel E. Rosner and David E. Keyes	None
	10. Work Unit No.
	None

9. Performing Organization Name and Address	11. Contract or Grant No.
Yale University Dept. of Chemical Engineering and Mechanical Engineering New Haven, Connecticut 06520	NAG3-898
	13. Type of Report and Period Covered Contractor Report Final

12. Sponsoring Agency Name and Address	14. Sponsoring Agency Code
National Aeronautics and Space Administration Lewis Research Center Cleveland, Ohio 44135-3191	

15. Supplementary Notes

Project Managers: Gary D. Roberts and Thomas K. Glasgow, Materials Division, NASA Lewis Research Center.

16. Abstract

Results are reported of a preliminary theoretical study of the coupled mass-, momentum-, and heat-transfer conditions expected within small ampoules used to grow oriented organic solid (OS-) films, by physical vapor transport (PVT) in microgravity environments. It is shown that previous studies made restrictive assumptions (e.g., smallness of $\Delta T/T$, equality of molecular diffusivities) not valid under PVTOS conditions, whereas the important phenomena of sidewall gas 'creep', Soret transport of the organic vapor, and large vapor phase supersaturations associated with the large prevailing temperature gradients were not previously considered. Rational estimates are made of the molecular transport properties relevant to copper-phthalocyanine monomeric vapor in a gas mixture containing H_2(g) and Xe(g). Efficient numerical methods have been developed and are outlined/illustrated here for making steady axisymmetric gas flow calculations within such ampoules, allowing for realistic $\Delta T/T_w$-values, and even corrections to Navier-Stokes-Fourier 'closure' for the governing 'continuum' differential equations. High priority follow-on studies are outlined based on these new results.

17. Key Words (Suggested by Author(s))	18. Distribution Statement
Convection; Vapor deposition; Molecular transport; Boundary conditions; Microgravity	Unclassified – Unlimited Subject Category 34

19. Security Classif. (of this report)	20. Security Classif. (of this page)	21. No of pages	22. Price*
Unclassified	Unclassified	54	A04

NASA FORM 1626 OCT 86

*For sale by the National Technical Information Service, Springfield, Virginia 22161